

High-throughput screen to identify compounds that prevent or target telomere loss in human cancer cells

Chris Wilson¹ and John P. Murnane^{1,2,*}

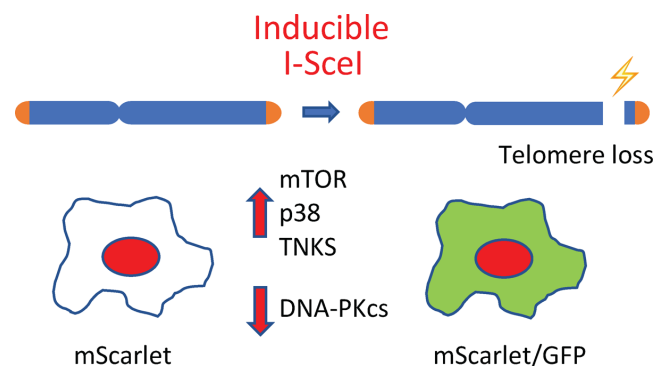
¹Department of Pharmaceutical Chemistry, Small Molecule Discovery Center, University of California, San Francisco, CA 94143, USA and ²Department of Radiation Oncology, University of California, San Francisco, CA 94143, USA

Received June 27, 2022; Revised September 09, 2022; Editorial Decision September 14, 2022; Accepted September 29, 2022

ABSTRACT

Chromosome instability (CIN) is an early step in carcinogenesis that promotes tumor cell progression and resistance to therapy. Using plasmids integrated adjacent to telomeres, we have previously demonstrated that the sensitivity of subtelomeric regions to DNA double-strand breaks (DSBs) contributes to telomere loss and CIN in cancer. A high-throughput screen was created to identify compounds that affect telomere loss due to subtelomeric DSBs introduced by I-SceI endonuclease, as detected by cells expressing green fluorescent protein (GFP). A screen of a library of 1832 biologically-active compounds identified a variety of compounds that increase or decrease the number of GFP-positive cells following activation of I-SceI. A curated screen done in triplicate at various concentrations found that inhibition of classical nonhomologous end joining (C-NHEJ) increased DSB-induced telomere loss, demonstrating that C-NHEJ is functional in subtelomeric regions. Compounds that decreased DSB-induced telomere loss included inhibitors of mTOR, p38 and tankyrase, consistent with our earlier hypothesis that the sensitivity of subtelomeric regions to DSBs is a result of inappropriate resection during repair. Although this assay was also designed to identify compounds that selectively target cells experiencing telomere loss and/or chromosome instability, no compounds of this type were identified in the current screen.

GRAPHICAL ABSTRACT



INTRODUCTION

Chromosome instability (CIN) plays an important role in carcinogenesis by contributing to an increased mutation rate that leads to tumor cell progression and resistance to anti-cancer therapy (1). CIN is an early event in most cancers and can arise through a number of different mechanisms (2), including oncogene-induced replication stress, which causes chromosome breaks at fragile sites (3). The investigation of CIN is therefore essential, not only to fully understand the cancer process, but to develop therapies to specifically target and kill cancer cells with CIN.

The ends of chromosomes, called telomeres, play a critical role in preventing CIN (4,5). Telomeres are composed of a 6 base-pair repeat sequence, which along with associated proteins called the shelterin complex, protect the ends of the chromosomes and keep them from appearing like DNA double-strand breaks (DSBs) (6,7). Telomere dysfunction is common in cancer cells and has been associated with CIN (8–11). Using plasmids integrated adjacent to telomeres, we have investigated the consequences and mechanisms of spontaneous telomere loss and its role in CIN for individual chromosomes in human cancer cells. One of the cell clones used in these earlier studies was derived from EJ-30, a bladder cell carcinoma cell line also known as MGH-U1 (12). EJ-30 is ideal for monitoring CIN in individual chromosomes, since despite being a p53-deficient cancer cell

*To whom correspondence should be addressed. Tel: +1 415 680 4434; Email: john.murnane@ucsf.edu

line, it has a relatively stable genome with 46 chromosomes (13–15).

Our results have shown that spontaneous telomere loss results in the fusion of sister chromatids (13–15), which then break during the subsequent mitosis and fuse again in the next cell cycle. These breakage-fusion-bridge (B/F/B) cycles continue for many cell generations, resulting in gene amplification and extensive gross chromosome rearrangements (GCRs) (14,15). B/F/B cycles continue until the chromosome acquires a new telomere, which often occurs by nonreciprocal translocation (15). Although telomere acquisition by nonreciprocal translocation stabilizes the chromosome that lost its telomere, it passes the instability on to the donor chromosome that gives up a telomere, and therefore the loss of a single telomere can eventually result in CIN involving multiple chromosomes.

Using this same telomeric plasmid system in combination with DSBs induced by I-SceI endonuclease, we have demonstrated that subtelomeric regions are highly sensitive to DSBs. This sensitivity is evident from the observation that I-SceI-induced DSBs at subtelomeric sites result in a much greater frequency of large deletions and GCRs than DSBs at interstitial sites (16–19). Importantly, this sensitivity to DSBs involves telomere loss and CIN similar to that seen with spontaneous telomere loss, as shown by both chromosome painting and DNA analysis in both mouse ES cells (20) and human cancer cells (19). This observation led to the proposal that spontaneous telomere loss in cancer cells results from a combination of the sensitivity of telomeric regions to DSBs, and a high frequency of DSBs near telomeres in cancer cells due to oncogene-induced replication stress (5).

The sensitivity of telomeric regions to DSBs is also evident from the persistence of ionizing radiation induced-DSBs in telomeric regions in nondividing primary human fibroblasts, which remain long after DSBs at interstitial sites have been repaired (21,22). This observation led Hewitt *et al.* to propose that the sensitivity of telomeric regions to DSBs is an important mechanism for protecting against CIN by promoting cellular senescence (22). However, unlike normal cells, our results demonstrate that in human cancer cells the sensitivity of subtelomeric regions to DSBs has the opposite effect and promotes CIN, likely due to the lack cell cycle regulation, and therefore this sensitivity to DSBs plays an important role in CIN in human cancer (5).

The sensitivity of subtelomeric regions to DSBs provides the opportunity to investigate the cellular pathways involved in DSB repair and the mechanisms of formation of DSB-induced mutations. There are multiple pathways for repair of DSBs (23,24). The most common pathway for repair of DSBs in mammalian cells is C-NHEJ, which involves rejoining broken DNA ends. C-NHEJ utilizes the DNA-PK holoenzyme, which contains Ku70 and Ku80, which bind the free DNA ends to prevent resection (25,26), and DNA-PKcs, a large PI3K-related kinase whose signaling is important in the DDR and DSB repair (25,27,28).

A second option for DSB repair is homology-directed repair (HDR). Unlike C-NHEJ, HDR does not usually result in a mutation. However, HDR is limited to the S/G2 phases of the cell cycle, after DNA replication and before chromatin condensation, since it requires the adjacent sis-

ter chromatid as a template. HDR is initiated by binding of the MRE11/RAD50/NBS1 (MRN) complex to the DSB, which leads to activation of ATM, another PI3K-like kinase involved in the DDR (29). ATM is involved in protecting the break through the activation of 53BP1 (30), as well as initiating resection in S/G2 to generate a 3' single-stranded DNA overhang used for HDR (31). Importantly, the resection at the DSB prevents C-NHEJ, which is unable to rejoin resected ends (32–35). Therefore, once HDR has been initiated at a DSB, C-NHEJ can no longer occur.

A third DSB repair pathway, alternative end-joining (Alt-EJ, also called backup DSB repair and microhomology mediated repair) can rejoin short and long single-stranded overhangs utilizing sites of microhomology (36–40). Alt-EJ has often been considered to be a backup repair pathway in the absence of C-NHEJ or HDR, and is associated with the formation of large deletions and GCRs (37,38,41–43). However, Alt-EJ involving Pol θ primarily results in small deletions in the absence of defects in other DSB repair pathways, and therefore has been proposed to be important in maintaining chromosome stability (44–46).

We have previously investigated the mechanism responsible for the sensitivity of subtelomeric regions to DSBs. The focus of these studies was to attempt to understand how the proximity of telomeric repeat sequences and shelterin proteins influence the efficiency of DSB repair. The importance of telomeric repeat sequences in the sensitivity of telomeric regions to DSBs is evident from our results demonstrating a high frequency of large deletions at DSBs located near interstitial telomeric repeat sequences (17). Consistent with this observation, it was found that tethering the TRF2 shelterin protein near an interstitial DSB resulted in a deficiency in DSB repair, leading to the conclusion that TRF2 inhibits C-NHEJ (21). Importantly, we have shown that the sensitivity to DSBs extends at least 100 kb from a telomere (16). Moreover, as we have previously pointed out (4), the subtelomeric region that is sensitive to DSBs may be much larger than 100 kb based on the estimation of target size from the dose of ionizing radiation previously used to demonstrate persistent DSBs near telomeres in normal human cells (21,22).

Based on an earlier report that ATM is inhibited by TRF2 (47), we previously investigated whether a deficiency in ATM might be responsible for the sensitivity of telomeric regions to I-SceI-induced DSBs. The knockdown of ATM, or inhibition of ATM with KU55933, resulted in an increase in large deletions at interstitial DSBs (18). However, this increased frequency of large deletions was nowhere near that observed at subtelomeric DSBs. The results also showed that ATM is active near telomeres, because the inhibition of ATM caused a further increase in large deletions at subtelomeric DSBs. It was therefore clear that the sensitivity of subtelomeric regions to DSBs was not due to a deficiency in ATM. Our observation that ATM is active in response to subtelomeric DSBs is consistent with a subsequent study showing that ATM is active in response to DSBs in telomeric repeat sequences (48).

Due to its importance in resection of DSBs, we subsequently investigated the role of MRE11 in the sensitivity of subtelomeric regions to I-SceI-induced DSBs, using both knockdown with shMRE11 and inhibition of MRE11 exonuclease activity with Mirin (49). Our results showed that

inhibition of MRE11 exonuclease activity reduced the frequency of large deletions and GCRs, both at interstitial and telomeric DSBs, demonstrating a role for MRE11 in the formation of large deletions and GCRs at both locations.

The current study involves the development of an assay to identify proteins that either promote, inhibit or target telomere loss and CIN resulting from an I-SceI-induced subtelomeric DSB. This assay is only possible because of the high frequency of large deletions and GCRs at subtelomeric DSBs, although the proteins identified will likely provide information on mechanisms involved in the formation of rearrangements at interstitial DSBs. Telomere loss following the activation of I-SceI is detected as a result of the loss of a tet-repressor (TetR) gene adjacent to the telomere, which results in the expression of a gene for green fluorescent protein (GFP) located at another location (Figure 1). The cell clone used in this assay was derived from an EJ-30 cell clone previously used to monitor the consequences of the loss of a telomere (13–19). This assay was used in an unbiased high-throughput screen whose purpose was twofold. First, to learn more about the mechanism of sensitivity of subtelomeric regions to DSBs, and thus, the mechanisms of mis-repair of DSBs and CIN. Second, to identify compounds that can target proteins important in DSB repair and CIN that may be useful for cancer therapy, by either preventing telomere loss and CIN, or by selectively killing cells that have undergone telomere loss and/or CIN.

A screen of a library of 1832 biologically-active compounds using this assay identified a variety of compounds that could either increase or decrease the frequency of GFP-positive cells following the introduction of DSBs through the activation of I-SceI. The results demonstrate that inhibition of DNA-PKcs increases the frequency of DSB-induced telomere loss, and therefore contrary to a previous report (21), a deficiency in C-NHEJ cannot explain the sensitivity of telomeric regions to DSBs. The inhibition of DNA-PKcs also greatly increases the frequency of small deletions at the I-SceI site, demonstrating that small deletions at the I-SceI-induced DSB are formed through Alt-EJ, and that Alt-EJ, like C-NHEJ, is important in preventing DSB-induced telomere loss. Finally, the results show that inhibition of mTOR, p38 and tankyrase decrease the frequency of telomere loss resulting from subtelomeric DSBs, demonstrating that these proteins contribute to the sensitivity of subtelomeric regions to DSBs. No compounds that selectively target cells experiencing telomere loss and/or chromosome instability were identified in this screen, although modifications of the assay are proposed to improve the chances of identifying this type of compound in future screens with larger compound libraries.

MATERIALS AND METHODS

Plasmids

Four different stably-integrated plasmids were used in this study. The first, pBS-TREx-GFP-hph, contains the gene for GFP under the control of a promoter that is regulated by the tetracycline-repressor protein (TetR) (Figure 1A). To construct this plasmid, the GFP gene, with a minimal cytomegalovirus (CMV) promoter and TetR binding sites immediately upstream, was excised from the pPRIME-TREX-

GFP-FF3 plasmid (50) and inserted into a Bluescript plasmid containing a hygromycin-resistance gene, pBS-hph-PA.

The second plasmid, pIRT-PEST-tel (Figure 1A), contains the gene for TetR with a recognition site for I-SceI endonuclease inserted on one end and telomeric repeat sequences inserted on the other end. pIRT-PEST-tel was derived from the plasmid pcDNA6/TR (ThermoFisher), which contains the TetR gene under the control of a CMV promoter, as well as a gene for resistance to blasticidin. A PEST sequence, which targets proteins for rapid degradation (51), was inserted in-frame at an *EcoRI* site near the C-terminal of the TetR gene to reduce its half-life and shorten the assay response time. The I-SceI recognition site used to introduce DSBs with I-SceI endonuclease (16–19,49) was inserted in a linker at a *NotI* site between the TetR gene and blasticidin-resistance gene. Eight-hundred base pairs of telomeric repeat sequences excised from plasmid pSX-neo1.6T2AG3 (52) were inserted at the end of the TetR gene opposite the I-SceI site, and were oriented so that they seed the formation of a new telomere following integration, as we have previously described (13–19,49). Importantly, the ampicillin-resistance gene and plasmid origin of replication in pIRT-PEST-tel is the same as that found in the pNCT-tel plasmid located immediately adjacent to a telomere on the long arm of chromosome 16 in cell clone B3-4 (13–15). This homology was used to target and replace the pNCT-tel plasmid with the pIRT-PEST-tel by homologous recombination, as has been previously performed by us with other plasmids in clone B3-4 (16,17,19).

The third plasmid, ddSceGR (not shown, kindly provided by Dr Simon Powell, Sloan Kettering), contains an inducible gene for a modified I-SceI endonuclease that can be activated by the addition of two separate agents, one that allows for transport into the nucleus (Triamcinolone Acetonide, TA), and the other for increased stability (Shield1, Sh1) (53). ddSceGR also contains the Neo gene for selection with G418.

The fourth plasmid, pGK-puro-3xnls-mScarlet-I (not shown), contains a constitutively-expressed gene for mScarlet that contains three tandem nuclear localization signals (54). The mScarlet-labeled nuclei were used to monitor cell number. Nuclear localization was used because in our initial attempt using whole-cell labeling, the automated system was unable to accurately determine cell number as the cells became confluent. The 3xnls-mScarlet portion of the plasmid was derived from 3xnls-mScarlet-i (Addgene), and was inserted into the pPGKpuro plasmid containing the puro gene for selection.

Cell line

The mS11fs clone used in this assay contains the four different stably-integrated plasmids described above, which were used to detect telomere loss following the introduction of a subtelomeric DSB. Telomere loss in clone mS11fs was detected by loss of the adjacent TetR gene, which results in expression of GFP (Figure 1A). mS11fs was derived from clone B3-4 of the bladder cell carcinoma cell line, EJ-30, also known as MGH-U1 (12). B3-4 contains the pNCT-tel plasmid integrated at the end of the long arm of chromosome 16 and has been used extensively to analyze how

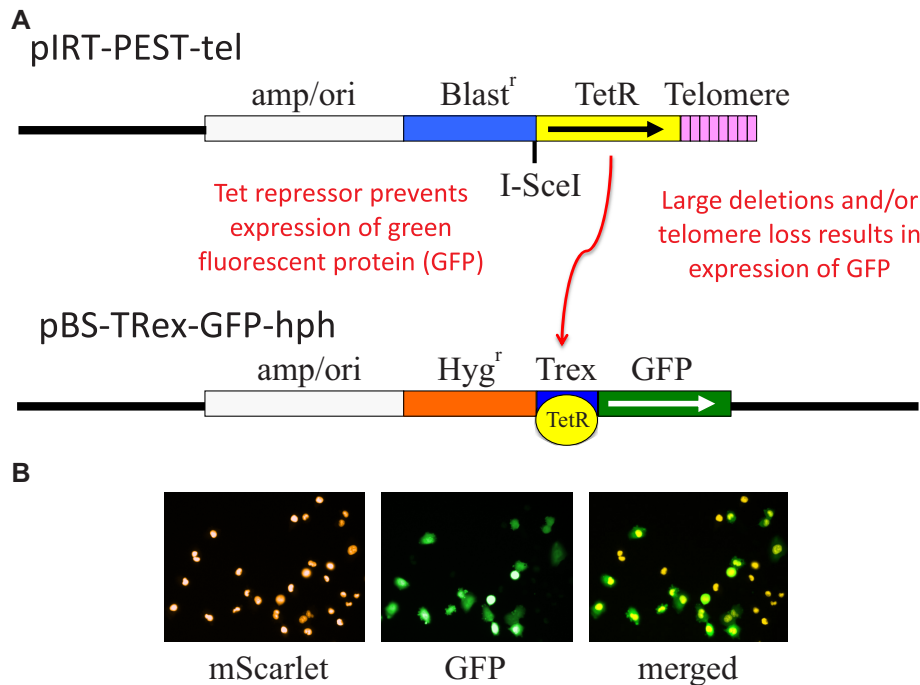


Figure 1. Two of the plasmids integrated in cell clone mS11fs that are used to monitor DSB-induced telomere loss. (A) An I-SceI endonuclease-induced DSB within the pIRT-PEST-tel plasmid located adjacent to a telomere results in loss of the distal TetR gene and telomere. The loss of the TetR gene results in expression of the GFP gene controlled by a TRex promoter in the pBS-Trex-GFP-hph plasmid integrated at another location. Clone mS11fs also contains (not shown) the stably-integrated ddSceGR plasmid containing a gene for inducible I-SceI, and the pGK-puro-3xnl-mScarlet-i plasmid containing a gene for the constitutively-expressed nuclear mScarlet that is used to control for cell number. (B) Images of constitutive mScarlet-labeled nuclei (red), GFP-labeled cells following treatment with TA/Sh1 (green), and merged mScarlet and GFP-labeled cells.

both spontaneous (13–15) and DSB-induced (16–19,49,55) telomere loss influence CIN.

To create clone mS11fs, clone B3-4 was first transfected with plasmid pBS-Trex-GFP-hph, and hygromycin-resistant colonies expressing GFP were selected. Next, one of the hygromycin-resistant, GFP-positive clones was transfected with the pIRT-PEST-tel plasmid. As mentioned above, pIRT-PEST-tel shares homology with the pNCT-tel plasmid located at the telomere on chromosome 16 in clone B3-4, which facilitates targeted integration by homologous recombination. Targeted integration was achieved by first selecting with blasticidin for stable integration of pIRT-PEST-tel, followed by selection with ganciclovir for clones that had lost the pNCT-tel plasmid, which contains the HSV-tk gene that sensitizes cells to ganciclovir. Several GFP-negative clones resulting from the presence of the TetR repressor were then selected and the DNA analyzed by Southern blot using a probe specific for the TetR and blasticidin genes to determine whether the telomeric repeat sequences in pIRT-PEST-tel had become the new telomere on chromosome 16 (Supplementary Figure S1). As we have previously demonstrated, plasmids in which telomeric repeat sequences in the plasmid seed the formation of a new telomere are easily identified by the heterogeneity in the size of the bands due to the variability in telomere length (13). Unlike other bands, these diffuse bands are sensitive to Bal31 exonuclease, demonstrating that they are terminal telomeric repeats (13). Similar targeting by homologous recombination has previously been used by us to substitute other plasmids for the telomeric plasmid in clone B3-4

(16,17,19). Using this criteria, two clones, 8 and 11, contained the targeted pIRT-PEST-tel plasmid located at the telomere. These clones demonstrated GFP-positive sectors as colonies grew in size, as would be expected from spontaneous loss of the telomere containing the TetR repressor (data not shown), typical of telomeres in clone EJ-30 (13–15) and other cancer cells (8,9).

Next, one of the clones showing GFP-positive sectors was grown up and transfected with the ddSceGR plasmid, and G418-resistant colonies were selected. Several of these G418-resistant clones were then tested for the presence of the I-SceI gene by addition of TA (50 nM) and Sh1 (500 nM). One of the clones that showed a large increase in GFP-positive cells in response to TA/Sh1 was selected for further use. This clone was then transfected with the pGK-puro-3xnl-mScarlet-I plasmid, and selection was performed with puromycin. Clones containing nearly 100% bright mScarlet-labeled nuclei were selected for further use. One of these clones, mS11, was then subjected to flow sorting for GFP-negative cells to reduce the low level of GFP background caused by the spontaneous loss of the telomere. This clone, named mS11fs, was used for the assay in this study.

It is important to point out that with each of the four plasmids, individual clones were selected that showed maximum stability of the integrated plasmid and expression. With pBS-Trex-GFP-hph, this involved selecting for the clones with the brightest GFP that showed little if any variegation when the culture was expanded. With pIRT-PEST-tel, this involved selecting for clones in which GFP could be

induced rapidly in all cells following the addition of doxycycline to inactivate TetR. With pGK-puro-3xnlx-mScarlet-I, this involved selecting clones that continued to show bright mScarlet staining in nearly all nuclei in the population during expansion of the clone. Finally, with ddScGR, this involved screening for clones that upon expansion continued to show high levels of GFP-positive cells following the addition of TA/Sh1. Although re-selection is possible with all four of the plasmids, this has not been necessary to maintain their expression.

UCSF SMDC bioactive compound library and screen

The mS11fs cells used for the high-throughput screen were thawed two days before they were to be used. Following trypsinization, the trypsin was poured off and the cells resuspended in growth medium. The cells were then pipetted multiple times with a small-bore plastic pipette, counted, and pelleted by centrifugation. The cells were then suspended in 5 ml of ice-cold PBS containing Proteinase K (100 μ g/ml), and incubated 10 minutes on ice. Proteinase K treatment is necessary because without it the EJ-30 cells aggregate after trypsinization, which becomes an issue due to the prolonged time it takes to plate the cells for the screen. Following Proteinase K treatment, 5 ml of ice-cold PBS containing 1% Bovine Serum Albumin is added, and the cells pelleted by centrifugation. The cells were then resuspended at approximately 1×10^6 cells/ml and counted again. The cells were then diluted in ice-cold growth medium at 3750 cells/ml to provide the 150 cells in the 40 μ l aliquots used in the screen.

Cells were kept on ice until dispensed into 384 well optical (Greiner μ Clear) plates by a WellMate automated bulk dispenser, and incubated overnight at 37°C in an incubator in 5% CO₂. The day after plating TA (50 nM) and Sh1 (500 nM) in media were added to the wells of 6 of the plates (screen). Six other plates (counter) were not treated with TA and Sh1 and received media only. Pre-arrayed compounds (SelleckChem) at 1mM in 100% DMSO were then added by automated pin-tool (Beckman Coulter Biomek FXP) to a final concentration of 1 μ M (0.1% DMSO) in both the counter and screen plates to determine the effect of the compounds on the frequency of GFP-positive cells and cell number, with or without the addition of TA/Sh1. Each plate contained four columns of controls in which no compounds were added (columns 1, 2, 23 and 24), which consisted of cells either without TA/Sh1 (counter) or with TA/Sh1 (screen). Automated image acquisition (INCell 2500 high-content microscope) and analysis (INCell Developer Toolbox) were performed beginning one day after addition of the compounds (Day 1), followed by imaging and analysis on days 4, 5 and 6 after compound addition. Image analysis to determine cell number was performed by segmentation and counting of mScarlet-labeled nuclei (Figure 2).

Image analysis to determine the number of GFP-positive cells was performed by either determining the percent of GFP-positive cells relative to mScarlet-positive cells, or by multiplying the density and area of each GFP signal to get the intensity (DxA), and then summing up the total DxA for all GFP signals in an image. The total GFP DxA for

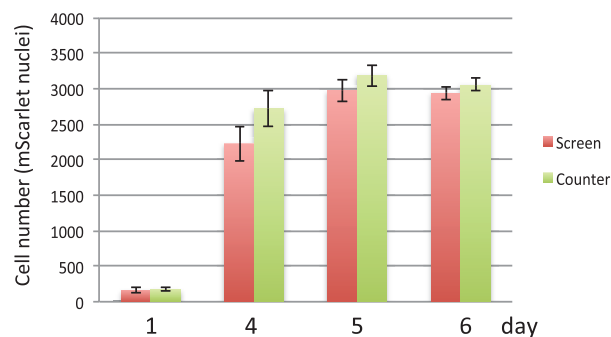


Figure 2. Analysis of cell number following growth with or without TA/Sh1. Cell number was determined by counting mScarlet-labeled nuclei in cells treated with (red, Screen) or without (green, counter) TA/Sh1. Cell growth was slightly slower in the TA/Sh1-treated cells at day 4 (P value < 0.0001), with no significant change in cell number after day 5. Error bars represent standard deviation.

each image was then normalized for cell number by dividing by the number of mScarlet-positive nuclei in the same image (Norm-GFP-Sum).

Low-intensity background GFP (low bin – grey scale intensity < 25 000), measured either as percent GFP-positive cells (%GFP+) or Norm-GFP-Sum, was often higher than the GFP signal observed in the TA/Sh1-treated cells due to low intensity background GFP (Supplementary Figure S2). This background GFP was greatly reduced when measuring mid-intensity GFP (mid bin – grey scale intensity 25 000–40 000) (Supplementary Figure S2), and nearly eliminated when measuring only high-intensity GFP (high bin – grey scale intensity > 40 000) (Figure 3). The subsequent analysis of the effect of compounds on the number of GFP-positive cells resulting from TA/Sh1, as presented below, is therefore adjusted for high-intensity GFP to eliminate background GFP. To accomplish this, the effect of the compound, with or without TA/Sh1, was determined by multiplying the Norm-GFP-Sum by the fraction of cells with high-intensity GFP (Norm-HI-GFP-Sum). The fold-change in the Norm-HI-GFP-Sum caused by the compound was determined by dividing the Norm-HI-GFP-Sum value in wells treated with the compound in combination with TA/Sh1 by the average Norm-HI-GFP-Sum of the control wells treated with TA/Sh1 alone in all six plates (384 wells). Norm-HI-GFP-Sum is used in the analysis below to represent the number of GFP-positive cells.

Analysis of compounds in the laboratory

The analysis of the effect of compounds on the frequency of GFP-positive cells in the laboratory was performed using a Cellometer K2 (Nexcelom), which has the capability of counting both GFP-positive and mScarlet-positive cells. The day prior to addition of compounds with or without TA/Sh1, 20K cells were added to triplicate six-well plates. The following day 4 ml of medium containing the various concentrations of test compounds with or without TA (50 nM) and Sh1 (500 nM). After incubating 5 days, cells were trypsinized, resuspended in 1 ml of medium and the number of GFP-positive and mScarlet-positive cells determined.

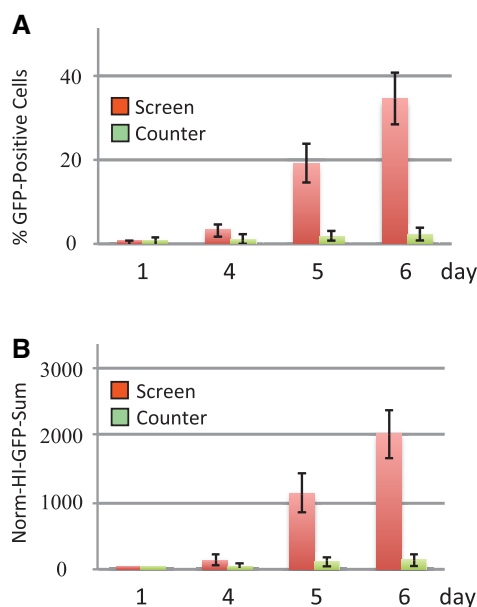


Figure 3. Analysis of high-intensity GFP-positive cells in control and TA/Sh1-treated wells. (A) The percent of high-intensity GFP-positive cells following addition of TA/Sh1 increased to 20% by day 5, and 35% by day 6, while background GFP remained nearly unchanged. (B) A similar increase in GFP-positive cells following TA/Sh1 treatment is observed by monitoring the combined high intensity GFP signal from all GFP-positive cells (Norm-HI-GFP-Sum, see Materials and Methods). Norm-HI-GFP-Sum is used in this study to represent the changes in high-intensity GFP-positive cells in the population. Error bars represent Standard Deviation.

Analysis of small deletions

The frequency of small deletions in cell clone GFP-7F2 were determined as previously described (17,18,49). Briefly, the frequency of small deletions induced by I-SceI was determined by performing PCR on genomic DNA from the total population of cells using two primers spanning the I-SceI site. Digestion of the PCR product with I-SceI is performed to determine the percentage of cells in the population that have lost the I-SceI, since the PCR product from cells in the population that have small deletions will not be cut by I-SceI. However, cells with large deletions or GCRs at the I-SceI site do not generate a PCR product, which results in an overestimation of the percentage of cells in the population that have small deletions. Therefore, the results must first be corrected by multiplying the percentage of uncut PCR product by the fraction of cells without large deletions or GCRs, as determined by the percentage of cells that have maintained expression of the GFP gene in the plasmid containing the I-SceI site.

The protocol involved plating 100K cells in duplicate T25 flasks. The following day, the compounds were added at 1 μ M (except for ATR inhibitor VE-822, at 500 nM) in combination with TA/Sh1. The cells were then grown for 12 days to allow for the generation of small deletions. The cells were split on day 4 and again on day 8, at which time they were transferred to a T75 flask. On the 12th day, the cells were harvested, DNA prepared using QIAmp DNA kit (Qiagen).

RESULTS

Initial screen of a library of 1832 compounds

Our initial screen involved the analysis of a library of 1832 known bioactive compounds at a concentration of 1 μ M, with or without the addition of TA/Sh1 to induce DSBs. Cell growth in control wells without test compounds, as measured by the number of mScarlet-positive nuclei, slowed after day 4 when cells became confluent (Figure 2), with no significant change in cell number between days 5 and 6. Cells treated with TA/Sh1 grew slightly slower than cells without TA/Sh1 at day 4, based on the average of 384 total wells from all six plates (2319 ± 251 TA/Sh1, 2728 ± 226 control, P value < 0.0001). Treatment with TA/Sh1 resulted in a large increase in high intensity GFP-positive cells, measured either as percent GFP-positive cells (GFP-positive/mScarlet-positive cell ratio, Figure 3A) or the total high-intensity GFP signal divided by the number of mScarlet-positive cells (Norm-HI-GFP-Sum, Figure 3B). Norm-HI-GFP-Sum, which accurately tracks the percent of GFP-positive cells, was selected for the analysis used in this study. Monitoring only high intensity GFP was necessary due to a background of low and mid-intensity GFP (Supplementary Figure S2). After an initial delay, $\sim 35\%$ of the cells expressed high intensity GFP by day 6 in the TA/Sh1-treated controls, while the increase in the percent of cells expressed high intensity GFP was negligible in controls without TA/Sh1. The initial delay in the increase in the number of cells expressing high intensity GFP following addition of TA/Sh1 was expected due to the time required for telomere loss, TetR turnover, and GFP expression. The large increase in the number of cells expressed high intensity GFP after treatment with TA/Sh1 is consistent with our earlier studies showing that telomeric regions are highly sensitive to DSBs (16–19,49). In contrast, as we (16–19,49) and others (56–59) have shown, I-SceI-induced DSBs at interstitial sites rarely produce large deletions or GCRs.

As expected, some compounds in the initial screen caused an increase in the Norm-high-GFP-Sum that was independent of treatment with TA/Sh1 (Supplementary Figure S3), and therefore did not result from loss of the TetR gene. The compounds that resulted in expression of GFP in nearly all of the cells by day 1 included tetracycline, doxycycline, and methacycline, which directly bind and inhibit the TetR protein (60). Due to the potency of these compounds, some carryover was also observed in the same wells in plates treated subsequently. Therefore, the results of the wells with a large increase in high intensity GFP-positive cells by day 1 (red rectangles) were not considered for further analysis. Importantly, no carryover was evident with any of the other test compounds in this screen.

Although it is also possible that some compounds could also increase the number of GFP-positive cells in the absence of TA/Sh1 by promoting telomere position effect (TPE), the silencing of genes near telomeres (61), this was not observed. We have previously reported that TPE actively silences telomeric transgenes in mouse ES cells (62). However, we have found that TPE is much less robust in silencing telomeric transgenes in human tumor cells (16), which has allowed us to stably express genes

for prolonged periods. To determine whether compounds produced a TA/Sh1-independent increase in the number of GFP-positive cells by enhancing TPE, we utilized cell clone GFP-6D1, which contains an expressed GFP gene located adjacent to a telomere (17–19,49). None of the compounds that caused a TA/Sh1-independent increase in GFP-positive cells had any effect on suppressing the expression of the telomeric GFP gene in clone GP-6D1 (data not shown).

The compounds in the library used in this study are well characterized as to their specific targets. However, as with any inhibitor, off-target effects are always a possibility. To increase the chances of identifying specific protein targets, compounds known to inhibit the same protein were grouped together in the initial screen analysis for comparison (Figure 4). The effect of the compounds in these groups on the Norm-HI-GFP-Sum in response to TA/Sh1 (fold-change) was then compared with the average of the Norm-HI-GFP-Sum in response to TA/Sh1 alone in the 384 control wells from all 6 plates. For the sake of comparison, the Norm-HI-GFP-Sum of the compounds is shown relative to the average of the Norm-HI-GFP-Sum in response to TA/Sh1 for all compounds, which was 1.2-fold higher (blue vertical line, Figure 4) than the average of the 384 control wells with TA/Sh1 alone.

No groups of compounds targeting a specific protein were found that consistently caused an increase in the Norm-HI-GFP Sum in response to TA/Sh1, although some individual compounds did, including etomidate and scriptaid (top panel, Figure 4). In contrast, multiple compounds targeting a specific protein were found that caused a decrease in the Norm-HI-GFP-Sum in response to TA/Sh1 (lower panels, Figure 4). Some of these groups of compounds target proteins that are involved in pro-growth pathways and/or resistance to cell stress (mTOR, p38, ALK). In addition, two compounds targeting the WNT pathway also caused a decrease in the Norm-HI-GFP-Sum in response to TA/Sh1 (Figure 4). With some groups of compounds targeting a specific protein (SRC, RAF), only a few compounds in the group caused a large decrease in the Norm-HI-GFP-Sum in response to TA/Sh1, suggesting off-target effects for these compounds.

An important observation made in the course of these studies is that the inhibition of cell growth by a compound can in itself decrease the Norm-HI-GFP-Sum in response to TA/Sh1. This is demonstrated by the results showing that compounds that significantly inhibited cell growth in the absence of TA/Sh1 invariably caused a decrease in the Norm-HI-GFP-Sum in cells treated with TA/Sh1 (Supplementary Figure S4). This result demonstrates that telomere loss resulting from subtelomeric DSBs requires cell division. Therefore, any decrease in the Norm-HI-GFP-Sum in response to TA/Sh1 that occurs at concentrations of compounds that inhibit cell growth in the absence of TA/Sh1 is not necessarily a result of telomere loss, which is addressed in greater detail below.

The initial screen identified a variety of compounds that were candidates for further analysis. As seen in Figure 4, our initial screen showed that many inhibitors of mTOR greatly decreased the Norm-HI-GFP-Sum in response to TA/Sh1, although some did not. Several of the mTOR in-

hibitors also inhibited cell growth, making it difficult to tell whether the decrease caused by these compounds was due to DSB-induced telomere loss. Four of the mTOR inhibitors that decreased the Norm-HI-GFP-Sum in response to TA/Sh1 with minimal impact on cell growth, temsirolimus, AZD2014, GDC-0349 and OSI-027, were chosen for further analysis in the follow-up screen (red circles, Figure 4).

All but one of the inhibitors of p38 caused a partial decrease in the Norm-HI-GFP-Sum in response to TA/Sh1 without impacting cell growth (Figure 4). The one exception was asiatic acid, which is not specific for p38 (63). Four of the p38 inhibitors, BIRB796, PH-797804, ralimetinib, and TAK-715, were chosen for further analysis in the follow-up screen.

Inhibitors of SRC and RAF varied considerably in their ability to decrease the Norm-HI-GFP-Sum in response to TA/Sh1 (Figure 4). Two of the SRC inhibitors, saracatinib and bosutinib, and one of the RAF inhibitors, AZ628, that caused a large decrease in the Norm-HI-GFP-Sum in response to TA/Sh1, but had a minimal effect on cell growth (red circles, Figure 4), were chosen for further analysis in the follow-up screen.

Two of the inhibitors of the WNT pathway caused a large decrease in the Norm-HI-GFP-Sum in response to TA/Sh1 with no apparent effect on cell growth (red circles, Figure 4). Importantly, unlike the other WNT pathway inhibitors in the screen, these two inhibitors, IWR-1-Endo and XAV-939, were the only two compounds that target the WNT pathway through inhibition of tankyrase 1 and 2 (64–66), suggesting that inhibition of tankyrase is responsible. IWR-1-Endo and XAV-939 were chosen for further analysis in the follow-up screen.

Similar to the inhibitors of p38, all of the inhibitors of ALK in the initial screen, ceritinib, crizotinib, AP26113, AZD3463, GSK1838705 and TAE684, caused a partial decrease in the Norm-HI-GFP-Sum in response to TA/Sh1 with no apparent effect on cell growth (Figure 4). The ALK inhibitors were not included in the follow-up screen.

Follow-up screen with the curated library

Based on the results of our initial screen, a curated library of 37 compounds was generated for a more in-depth analysis. The follow-up screen with this curated library was conducted in triplicate at 2-fold dilutions at concentrations ranging from 1 μ M to 7.8 nM (Figure 5A and B). Many of the compounds selected for the curated library were those in the groups of compounds mentioned above that caused a decrease in the Norm-HI-GFP-Sum in response to TA/Sh1 with minimal impact on cell growth (circled in red, Figure 4). Several compounds were also included that caused a moderate (sirtinol, EX-527 and beta-lapachone) or large (scriptaid and etomidate) increase in the Norm-HI-GFP-Sum in response to TA/Sh1. In addition, compounds were included that are known to influence the DDR and DSB repair (inhibitors of ATM, DNA-PKcs). Finally, compounds were included that appeared to preferentially inhibit the growth of TA/Sh1-treated cells, including 10058-F4, ENMD-2076, NSC405020 and NSC697923. These compounds were of interest because they might selectively kill

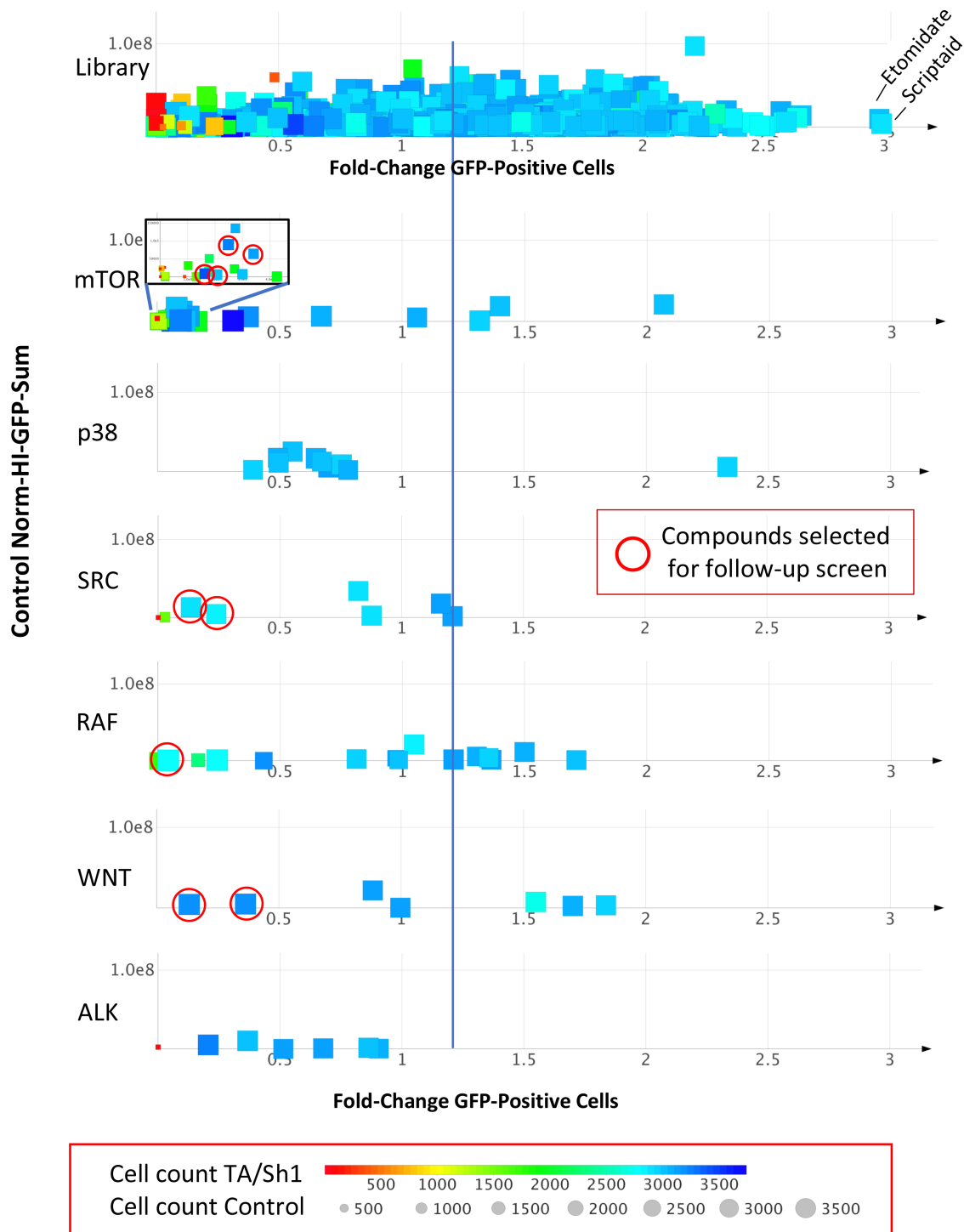


Figure 4. The effect that selected groups of compounds that target specific proteins have on the fold-change in the number of GFP-positive cells at day 6 in the initial screen. **(Top)** The fold-change caused by all of the compounds in the library (Library) on the number of GFP-positive cells in response to TA/Sh1 (x axis) is demonstrated by dividing the Norm-HI-GFP-Sum in the screen (wells treated with compounds and TA/Sh1) by the average of the Norm-HI-GFP-Sum of the 384 control wells (all 6 plates) treated with TA/Sh1 alone. The fold-change values are plotted against the Norm-HI-GFP-Sum from cells treated with the compounds alone without TA/Sh1 to control for the effect of the compounds in the absence of TA/Sh1 (y axis). **(Bottom)** The results for compounds that target specific proteins (mTOR, p38, SRC, RAF, WNT, ALK) were grouped together for comparison. The cell counts in the wells treated with (Cell count Control, marker size) or without (Cell count TA/Sh1, marker color) TA/Sh1 are indicated, as is the average Norm-HI-GFP-Sum for all of the compounds tested (vertical blue line). Markers circled in red indicate specific compounds that were analyzed in the curated follow-up screen.

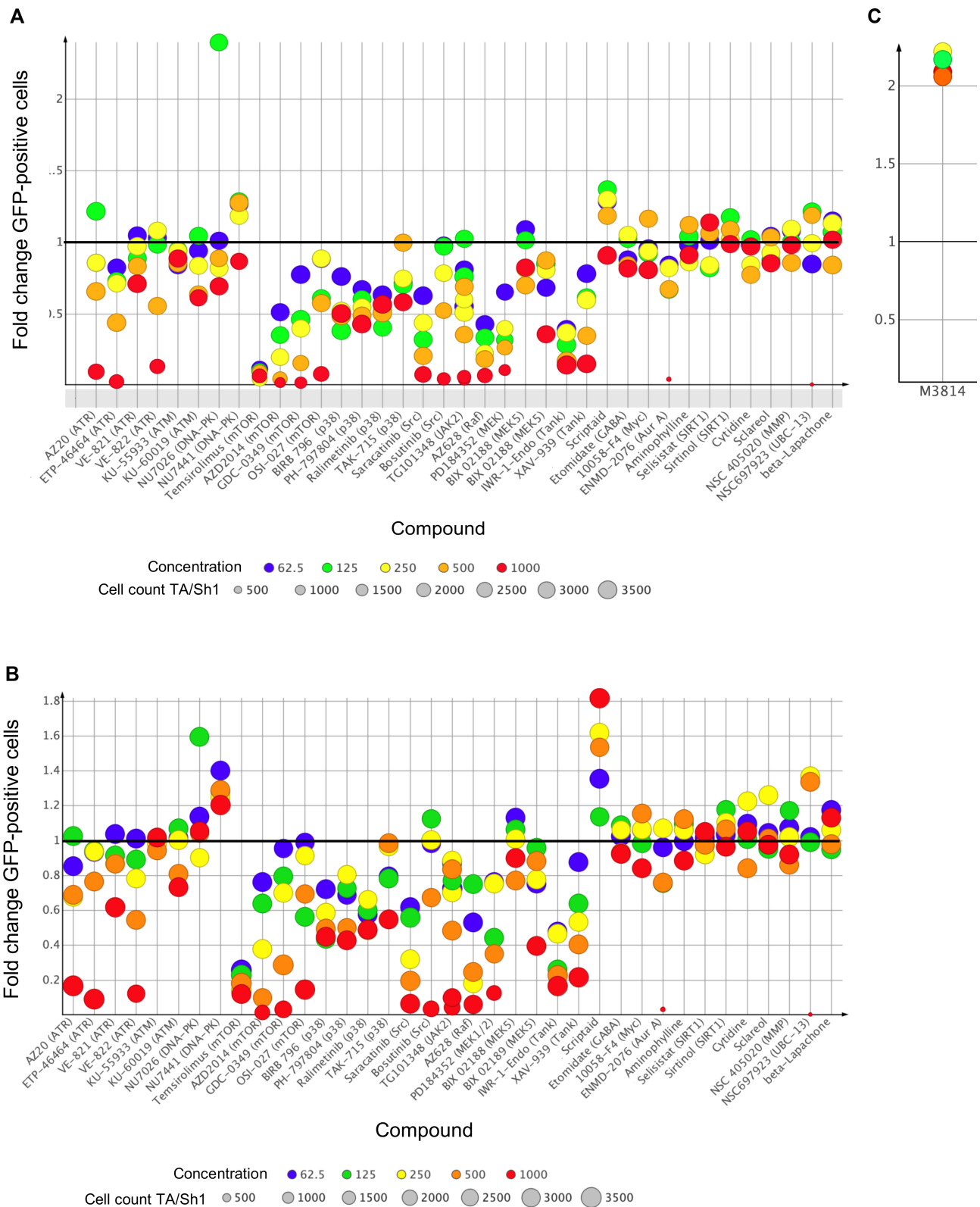


Figure 5. Effect of compounds in a curated follow-up screen on fold-change in GFP-positive cells in response to TA/Sh1. Fold-change in GFP-positive cells was determined by dividing the Norm-HI-GFP-Sum in wells treated with both the compound and TA/Sh1 by the average Norm-HI-GFP-Sum of the 192 control wells (3 plates) treated with TA/Sh1 alone. The screen was performed in triplicate with treatment at the different concentrations indicated. The compounds in the curated library were added with or without TA/Sh1 for (A) 5 days or (B) 6 days at concentrations of 1000 (red), 500 (orange), 250 (yellow), 125 (green), and 62.5 nM (blue). (C) The results of a follow-up assay performed in the laboratory with M3418, a DNA-PKcs-specific inhibitor. The influence of the compounds on the growth of cells (Cell count TA/Sh1) treated with TA/Sh1 is indicated by marker size. Compound TG101348 was tested twice, and the results of both tests are included for comparison.

cells that have undergone telomere loss and/or CIN, and therefore be of use in cancer therapy.

Compounds that decrease the norm-HI-GFP-sum in response to TA/sh1

The curated follow-up screen confirmed that the four mTOR inhibitors, temsirolimus, AZD2014, GDC-0349 and OSI-027 (67–70), all decrease the Norm-HI-GFP-Sum in response to TA/Sh1 (Figure 5). These compounds were included in the curated library because they showed minimal effects on cell growth in the initial screen at 1 μ M. However, in the follow-up screen some inhibition of growth was apparent with these compounds (Supplementary Figure S5), especially with temsirolimus, which inhibited cell growth at all of the concentrations tested down to 7.8 nM in the absence of TA/Sh1 (see arrows in mTOR panel, Supplementary Figure S5). Dose-response curves were generated to determine the IC₅₀ for the decrease the Norm-HI-GFP-Sum in response to TA/Sh1 for these compounds for comparison with their previously reported IC₅₀ values with their known targets (Figure 6). These comparisons were made with IC₅₀ values derived from the other studies using cultured cells (Table 1), since the IC₅₀ values obtained in cell-free systems are typically much lower due to factors such as uptake and degradation of the compounds (69,71). However, IC₅₀ values in cultured cells can also vary considerably depending on cell type and times of treatment.

The dose-response curve for the mTOR inhibitor, AZD2014 (Figure 6), demonstrated an IC₅₀ of 69 nM for the decrease in the Norm-HI-GFP-Sum in response to TA/Sh1 (Table 1), which is lower than the IC₅₀ for inhibition of TORC1 in cultured cells, 210 nM (72). Similarly, the dose-response curve for the mTOR inhibitor, GDC-0349 (Figure 6), demonstrated an IC₅₀ of 142 nM (Table 1), which is lower than the EC₅₀ for the anti-proliferative activity of GDC-0349 with a prostate cancer cell line, 310 nM (69). These dose-response curves also show that these inhibitors of mTOR are capable of causing a decrease in the Norm-HI-GFP-Sum in response to TA/Sh1 that is independent of any effect on cell growth. mTOR is a key protein in promoting cell growth and survival and the cellular response to stress (73). mTOR expression also promotes DSB repair (74), and inhibition of mTOR results in down-regulation of critical HDR proteins (75).

The four p38 inhibitors, BIRB796, PH-797804, ralimetinib, and TAK-715 (76,77), were shown in the follow-up screen to cause a decrease in the Norm-HI-GFP-Sum in response to TA/Sh1 without any effect on cell growth (Figure 5, Supplementary Figure S5). The dose-response curves for the decrease the Norm-HI-GFP-Sum in response to TA/Sh1 for three of these p38 inhibitors, BIRB796, PH-797804, and ralimetinib (Figure 6) were used to compare IC₅₀ values in our assay with the IC₅₀ previously reported for inhibition of p38 in cultured cells. The IC₅₀ estimated for ralimetinib, 17 nM (Table 1), is lower than the IC₅₀ required for ralimetinib to sensitize cultured cells to bortezomib, 200–400 nM (78,79). The IC₅₀ estimated for BIRB796, 65 nM (Table 1), is lower than the IC₅₀ of BIRB796 required to inhibit various p38-dependent functions and sensitize cultured cells to bortezomib, 100 to 400

nM (80,81). The IC₅₀ estimated for PH-797804, 49 nM (Table 1), is somewhat higher than the IC₅₀ required to inhibit p38, 5–10 nM (71). The uniformity in the ability of the p38 inhibitors to decrease the Norm-HI-GFP-Sum in response to TA/Sh1 (Figures 5 and 6) with no impact on cell growth shows that p38 is likely to play a role in promoting telomere loss in response to subtelomeric DSBs. However, why this decrease is limited to approximately half of the cells is unclear. p38 is vital for cellular resistance to stress in p53-deficient cells and telomere dysfunction (82), although the absence of any effect on cell growth demonstrates that this the modulation of cell death by p38 is not involved.

One of the SRC inhibitors that caused a large decrease in the Norm-HI-GFP-Sum in response to TA/Sh1 in our initial screen (Figure 4), saracatinib (83,84), also produced a large decrease in the follow-up screen (Figure 5). Although saracatinib had some effect on cell growth at 1 μ M, lower concentrations had no apparent effect on cell growth (Supplementary Figure S5). The dose-response curve for saracatinib (Figure 6) showed an IC₅₀ of 86 nM (Table 1), which is comparable to the IC₅₀ for inhibition of SRC in cultured cells, 62.5 nM (85,86). These results confirm that saracatinib is capable of causing a decrease in the Norm-HI-GFP-Sum in response to TA/Sh1 that is independent of any effect on cell growth. However, in view of the fact that other SRC inhibitors had much less of an effect (Figure 4), off-target effects seem likely, possibly due to the ability of SRC inhibitors to target multiple proteins (86).

A RAF inhibitor that caused a large decrease in the Norm-HI-GFP-Sum in response to TA/Sh1 in our initial screen, AZ628 (Figure 4), also produced a large decrease in the follow-up screen (Figure 5). The dose-response curve for AZ628 (Figure 6) demonstrated an IC₅₀ of 40 nM (Table 1), which is comparable to the IC₅₀ for C-RAF, 29 nM and B-RAF, 105 nM, in cell-free assays (87). AZ628 had some effect on cell growth at 1 μ M, however, at lower concentrations no apparent effect on cell growth was observed (Supplementary Figure S5). AZ628 can therefore decrease the Norm-HI-GFP-Sum in response to TA/Sh1 in the absence of inhibition of cell growth. However, the fact that other RAF inhibitors varied considerably in their ability to decrease the Norm-HI-GFP-Sum in response to TA/Sh1 (Figure 4), makes it likely that this is an off-target effect. Consistent with this possibility AZ628 prevents activation of a number of different tyrosine protein kinases, including VEGFR2, DDR2, Lyn, FLT1 and FMS (87). It is interesting to note, however, that SRC and RAF are in the same pathway (88,89).

The follow-up screen confirmed that the two compounds that inhibit tankyrase, IWR-1-Endo and XAV-939, cause a large decrease in the Norm-HI-GFP-Sum in response to TA/Sh1 without any inhibition of cell growth (Figure 5, Supplementary Figure S5). The dose-response curve for IWR-1-Endo and XAV-939 (Figure 6) demonstrated that the IC₅₀ for the decrease in the Norm-HI-GFP-Sum in response to TA/Sh1 for IWR-1-endo is 33 nM, and that for XAV-939 is 212 nM (Table 1). This IC₅₀ value IWR-1-endo is lower than the IC₅₀ for inhibition of tankyrase by IWR-1-endo, 80 nM (90). The value for XAV-939 is much higher than the IC₅₀ for inhibition of tankyrase by XAV-939 in a cell-free system, 11 nM (65), however, the IC₅₀ is much

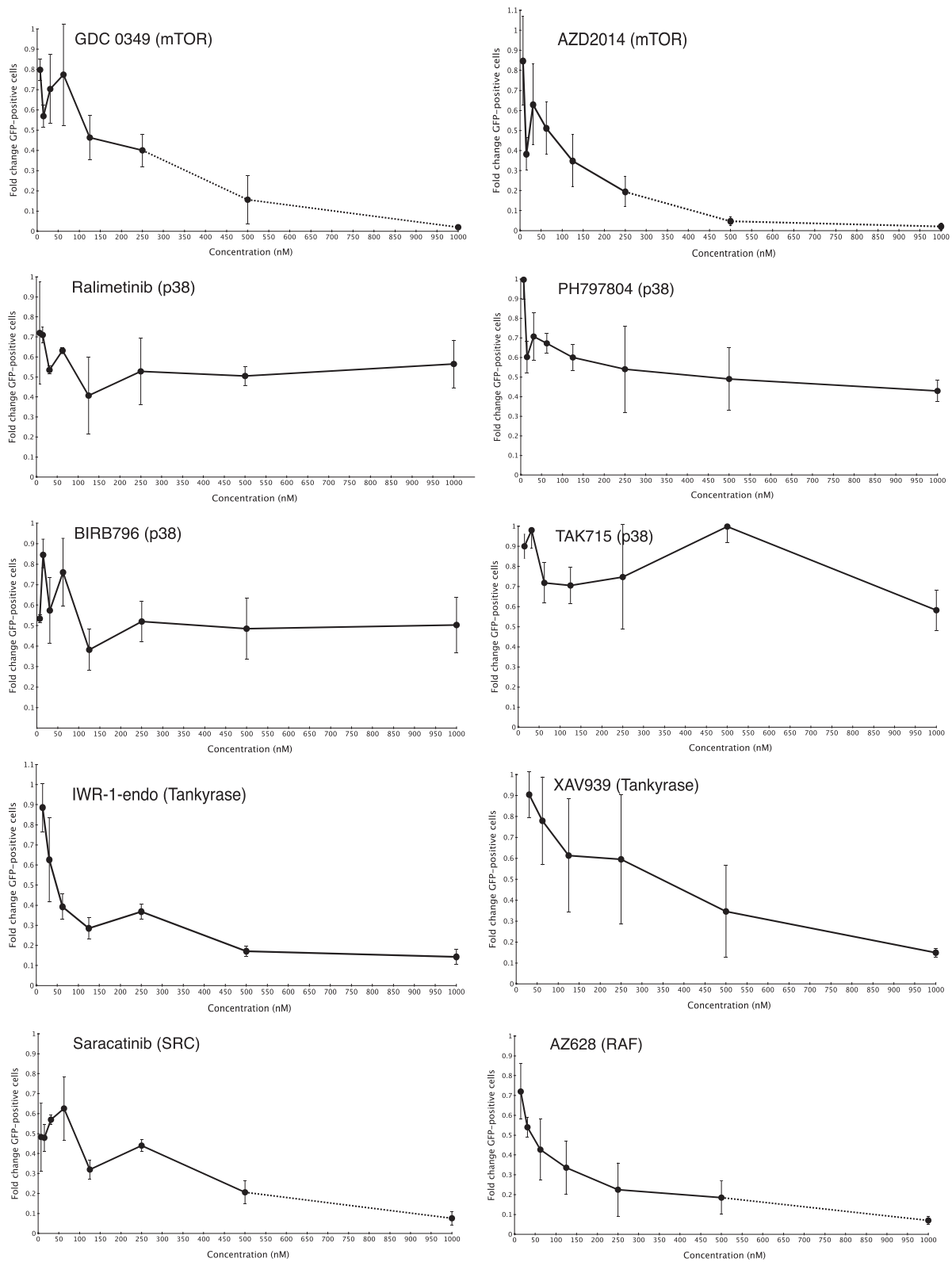


Figure 6. Dose response curves for the effect of various compounds in the follow-up screen on the fold-change of GFP-positive cells in response to TA/Sh1. Fold-change in GFP-positive cells was determined by dividing the Norm-HI-GFP-Sum in wells treated with both the compound and TA/Sh1 by the average Norm-HI-GFP-Sum of the 192 control wells (three plates) treated with TA/Sh1 alone. Graphs are shown for mTOR, p38, tankyrase, SRC and RAF inhibitors. The IC50 values were determined for each compound based on the maximum decrease observed in the Norm-HI-GFP-Sum using a four-parameter non-linear regression (see Table 1). Error bars represent Standard Deviation. Data points in which some growth inhibition by the compound (see Supplementary Figure S5) that would contribute to the decrease in the Norm-HI-GFP-Sum are indicated by dashed lines.

Table 1. IC50 values for the decrease in the Norm-HI-Sum-GFP in response to TA/Sh1

Target	Compound	Max % Inhib of GFP+ cells	Estimated IC50 (nM) ^δ	Published IC50 (nM) [∞]	Reference	Small deletions ^ψ
mTOR	AZ2014	99*	69	2.8/210	(78)	No effect
mTOR	GDC-0349	99*	142	5.5/310 ^ϕ	(75)	ND
p38	Ralimetinib	50	17	7/200 ^ξ	(84,85)	No effect
p38	PH-797804	50	49	5.8/5-10	(77)	No effect
p38	BIRB 796	50	65	0.1/100 ^ζ	(86,87)	ND
RAF	AZ628	92*	40	29 (C-RAF)	(93)	No effect
SRC	Saracatinib	92*	86	2.7/62.5	(91,92)	No effect
TNKS	IWR-1-endo	87	33	180	(96)	No effect
TNKS	XAV-939	85	212	11/1000 [§]	(71,97)	ND

^δEstimated IC50 is based on maximum level of inhibition observed with compound.

*Some inhibition of cell growth in controls without TA/Sh1.

[∞]IC50 in cell free system / IC50 in living cells.

[§]Concentration (not IC50) used for 12hrs to inhibit tankyrase in living cells.

^ϕKi for inhibitory potency and EC50 for anti-proliferative activity.

^ζConcentration required to inhibit the toxicity of bortezomib.

^ψEffect of compound on I-SceI-induced small deletions (ND, not determined).

less than the concentration of 1 μ M that was used to inhibit tankyrase in cultured cells (91). Importantly, IWR-1-Endo and XAV-939 stood out in this study in that they were the only two compounds that decreased the Norm-HI-GFP-Sum in response to TA/Sh1 by more than 80% in the absence of any effect on cell growth. It appears likely, therefore, that tankyrase plays a role in promoting telomere loss in response to subtelomeric DSBs. Tankyrase 1 and 2 have many functions (92), including stabilizing DNA-PKcs to promote C-NHEJ (91), and promoting HDR and cell cycle checkpoints in response to DSBs (93). In addition, tankyrase 1 has important roles at telomeres, where it is involved in terminating sister chromatid cohesion at telomeres after DNA replication (94) and regulating the addition of telomeric repeat sequences by telomerase (95).

Excluding possible artifacts as mechanisms for the decrease in the norm-HI-GFP-sum in response to TA/sh1

To confirm that the decrease in the Norm-HI-GFP-Sum in response to TA/Sh1 was a result of DSB-induced loss of the TetR gene, additional assays were performed to rule out that candidate compounds did not interfere with various aspects of the assay system. There are several ways that compounds could cause a decrease in the Norm-HI-GFP-Sum in response to TA/Sh1 other than the loss of the TetR gene. First, as discussed above, a decrease in the Norm-HI-GFP-Sum in response to TA/Sh1 could result from the inhibition of cell growth, because cell division is required for DSB-induced telomere loss. Second, it could result from the inhibition of expression of the GFP gene. Third, it could result from the inhibition of formation of I-SceI-induced DSBs, either by inhibiting I-SceI endonuclease directly, or by interfering with activation of I-SceI by inhibiting uptake or activity of TA and Sh1.

Although it is clear that the inhibition of cell growth can cause a decrease the Norm-HI-GFP-Sum in response to TA/Sh1 (Supplementary Figure S4), the effects of compounds on cell growth have been minimized by considering only compounds in which a large decrease the Norm-HI-GFP-Sum in response to TA/Sh1 was observed at concen-

trations that had minimal impact on cell number (Figure 5, Supplementary Figure S5).

To rule out the possibility that compounds might decrease the Norm-HI-GFP-Sum in response to TA/Sh1 by inhibiting GFP expression, a subsequent analysis was performed in the laboratory using the EJ-30 cell clone GFP-7F1. As mentioned above, clone GFP-7F1 contains a constitutively-expressed GFP gene integrated at an interstitial site (17,18,49). After addition of various candidate compounds selected for the follow-up screen, no decrease in the number of GFP-positive cells was observed after 5 days of growth (data not shown). These compounds therefore do not inhibit GFP expression.

The possibility that the compounds in our follow-up screen might decrease the Norm-HI-GFP-Sum in response to TA/Sh1 by inhibiting the formation of DSBs by I-SceI was investigated by monitoring the effect of the compounds on the frequency of small deletions at the I-SceI site. We have been unable to directly measure the frequency of DSBs at the I-SceI site, most likely because the I-SceI-induced DSBs are repaired very quickly and are therefore present for only a very short period of time (96). However, small deletions can be used as a surrogate marker for I-SceI-induced DSBs (Figure 7A, Supplementary Figure S6). Unlike large deletions and GCRs that are much more frequent at subtelomeric DSBs than interstitial DSBs (17–19,49), small deletions occur at the same frequency at subtelomeric and interstitial DSBs (17–19,49). Therefore, small and large deletions resulting from I-SceI-induced DSBs must occur through different mechanisms. Small deletions therefore provide a separate endpoint for monitoring the consequences of I-SceI-induced DSBs that is independent of the mechanism involved in producing large deletions and GCRs. Moreover, small deletions at I-SceI sites do not lead to CIN and cell death.

The effect of compounds on the production of small deletions produced by I-SceI was analyzed in the cell clone GFP-7F1, which contains the plasmid pGFP-ISceI integrated at an interstitial site. Clone GFP-7F1 was previously used in our studies demonstrating that the frequency of small deletions was similar at interstitial and subtelom-

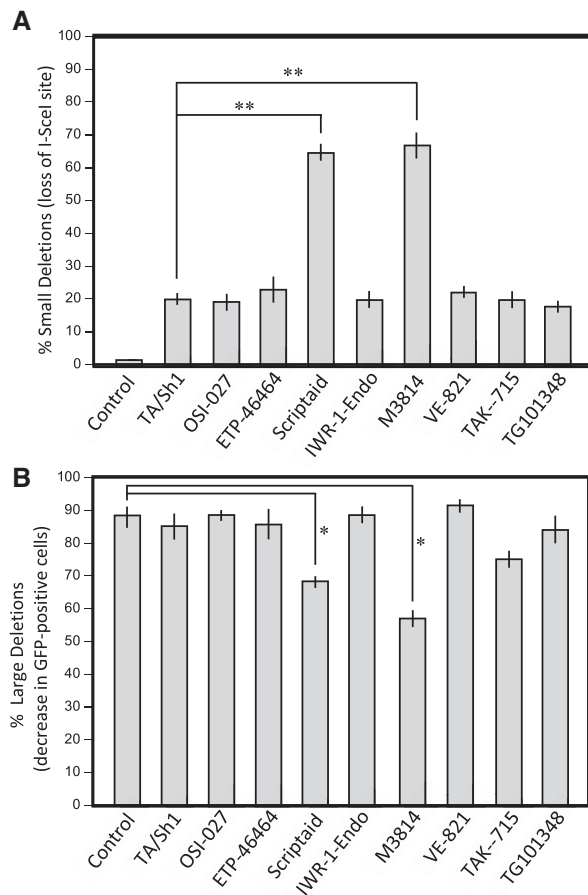


Figure 7. Effect of various compounds on the frequency of small and large deletions at an interstitial I-SceI in response to TA/Sh1. Cell clone GFP-7F1, which has an I-SceI site located between a constitutively expressed GFP gene and its promoter, was used to monitor both the frequency of small and large deletions at an interstitial I-SceI-induced DSB. (A) The percentage of cells with small deletions was determined from the fraction of a PCR product spanning the I-SceI site that cannot be cut with I-SceI (Supplementary Figure S7). (B) The frequency of large deletions and/or GCRs was determined from the increase in the percentage of cells that have lost GFP expression. Two separate experiments were performed using duplicate cultures in each. Error bars represent Standard Deviation. The data was analyzed using two-tailed *t*-test where (*) represents *P*-value < 0.005 and (**) represents *P*-value < 0.05.

eric DSBs (17–19,49). To measure small deletions, genomic DNA was isolated from cultures of clone GFP-7F1 following treatment TA/Sh1 for 12 days, and PCR was performed using primers that span the I-SceI site. The vast majority (99%) of the PCR product spanning the I-SceI site was cut by I-SceI endonuclease in control cells not treated with TA/Sh1 (Figure 7A, Supplementary Figure S6), demonstrating the absence of small deletions at the I-SceI site. The small percentage of the PCR product cut by I-SceI is likely due to a slight leakiness of the inducible I-SceI. In contrast, 20% of the PCR product was uncut in the cells treated with TA/Sh1, demonstrating the presence of small deletions at the I-SceI site in many cells in the population (Figure 7A, Supplementary Figure S6). Cells treated with the mTOR inhibitor OSI-027, the p38 inhibitor TAK-715, the JAK2 inhibitor TG101348, the ATR inhibitors ETP-46464 and VE-

822, and the tankyrase inhibitor IWR-1-endo all showed amounts of uncut PCR product similar to that of the cells treated with TA/Sh1 alone (Figure 7A, Supplementary Figure S6), demonstrating that these compounds had no effect on the production of I-SceI-induced small deletions. These compounds therefore do not inhibit the formation of I-SceI-induced DSBs. Similarly, other compounds in our studies that inhibit mTOR, p38, and SRC using concentrations that decrease the Norm-HI-GFP-Sum in response to TA/Sh1 were also found to have no effect on the frequency of I-SceI-induced small deletions (Table 1).

As we have previously reported (16–19), the results with clone GFP-751 also show that I-SceI-induced DSBs cause very few large deletions at interstitial sites, as seen by the fact that very few of the cells lose GFP expression as a result of the DSB between the GFP gene and its promoter (Figure 7B). Of the compounds tested, only inhibitors of DNA-PKcs caused an increase in large deletions at the interstitial I-SceI-induced DSB, which is discussed in more detail below.

Determining whether compounds that decrease the norm-HI-GFP-sum in response to TA/sh1 do so by preventing telomere loss or by eliminating cells that have undergone telomere loss

Compounds that decrease the Norm-HI-GFP-Sum in response to TA/Sh1 could do so by either reducing the frequency of DSB-induced telomere loss or by eliminating cells that have lost a telomere and/or have CIN. One method of distinguishing between these two possibilities is to determine whether the various compounds preferentially inhibit the growth of cells treated with TA/Sh1, which would be the case if the compounds selectively kill cells experiencing telomere loss and/or CIN. We therefore compared the effect of various compounds on the number of cells treated with or without TA/Sh1 (Figure 8). This analysis was performed using data obtained at day 5, since cells experiencing delayed growth might catch up to control cells by day 6 after control cells become confluent and stop growing at day 5 (see Figure 2). The difference in growth due to DSB-induced telomere loss would be limited to the number of cells that had lost a telomere by day 5. The number of GFP-positive cells at day 5 is 20% (see Figure 3A), which corresponds to ~35% of the cells having lost a telomere due to the delay in GFP expression. Therefore, if all of the cells experiencing telomere loss were selectively eliminated in the TA/Sh1-treated cells, then the maximum ratio of the number of control cells to TA/Sh1 treated cells would be 1.5 (100/65).

Comparison of the ratios of the number of cells in wells treated with the compound alone divided by the number of cells in wells treated with the compound plus TA/Sh1 demonstrated that some compounds preferentially inhibit growth in TA/Sh1-treated cells (Figure 8). This was most evident with the MEK1/2 inhibitor PD184352, which showed an increased ratio at all concentrations, although only the maximum ratio of 1.2 at 500 nM was significant (two-sided *t*-test *P*-value 0.028). These results were confirmed in the laboratory (data not shown). However, experiments in the laboratory also showed the same effect in cultures treated with TA alone, despite the fact that treatment with TA alone did not increase the Norm-HI-GFP-

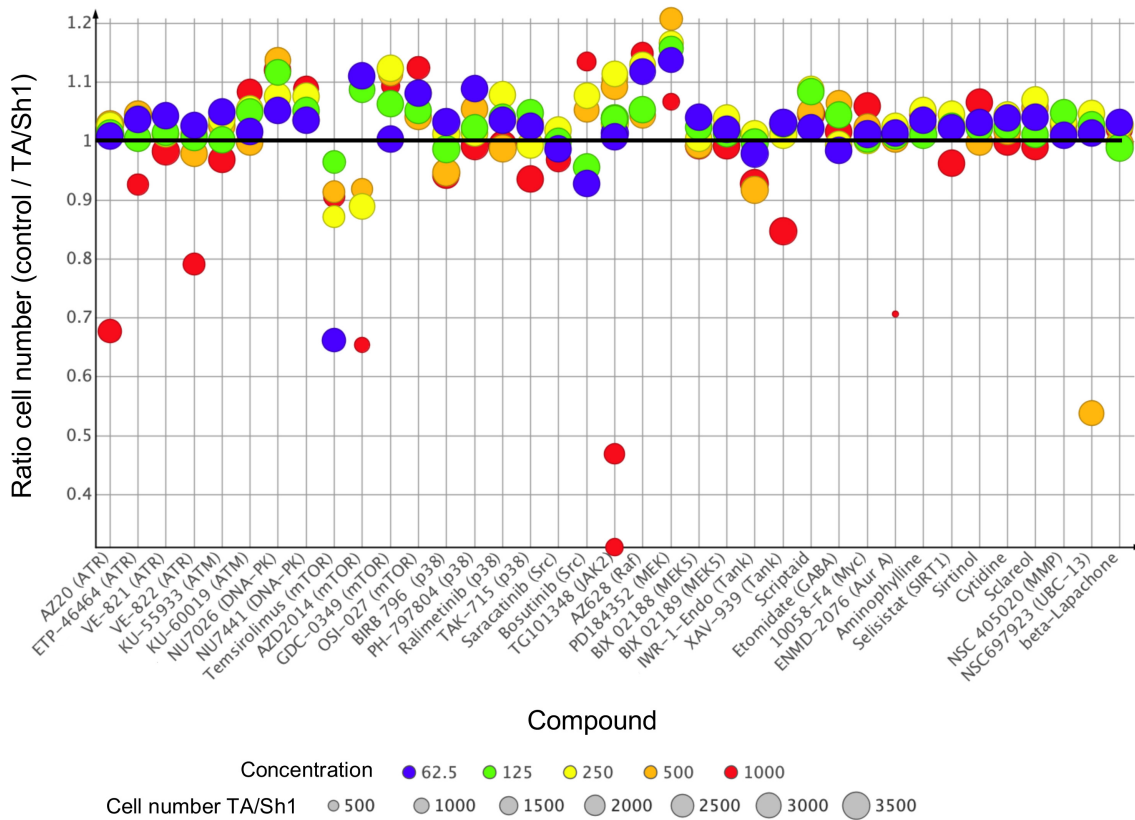


Figure 8. Comparison of the effects of compounds on cell growth with and without TA/Sh1. The ratio of the number of cells in the curated follow-up screen without and with TA/Sh1 (Control/Screen) at day 5 is shown for each of the compounds at different concentrations (marker color). The relative number of cells in the screen (with TA/Sh1) is indicated by marker size. Note that 35% of the cells will have lost a telomere by day 5, so that if a compound completely eliminates cells with telomere loss and/or CIN (GFP-positive cells), the ratio of the number of control to TA/Sh1-treated cells would be 1.5 (100/65).

Sum in response to TA/Sh1 (data not shown). The preferential inhibition of growth in TA/Sh1-treated cells with PD184352 therefore appears to be because TA sensitizes cells to PD184352, which indirectly reduces the Norm-HI-GFP-Sum in response to TA/Sh1 by inhibiting cell growth.

A small preferential inhibition of growth in TA/Sh1-treated cells was also seen with the RAF inhibitor AZ628, which was only significant at 1 μ M (two-sided t-test P-value 0.012). However, experiments in the laboratory with mS11f cells pretreated with TA/Sh1 for 3 days prior to addition of AZ628 showed no preferential elimination of GFP-positive cells. Therefore, AZ628 did not appear to show a preferentially toxicity in experiencing CIN as a result of telomere loss.

In addition to the compounds discussed above, other compounds that decreased the Norm-HI-GFP-Sum in response to TA/Sh1 and appeared to selectively inhibit the growth of TA/Sh1-treated cells in the initial screen were also included in the follow-up screen (Supplementary Figure S7). However, in the follow-up screen, 10058-F4 and NSC405020 had no effect on cell growth at any concentration, with or without TA/Sh1 (Figure 5), while ENMD-2076 and NSC697923 both nearly completely inhibited growth at 1 μ M (Figure 5), but this was not specific to TA/Sh1-treated cells (Figure 8).

Although not included in the follow-up screen, a number of other compounds in our initial screen gave results indicating that they may preferentially inhibit growth in cells treated with TA/Sh1 (see Supplementary Figure S7). Although several of these compounds were found to be false positives when tested in the laboratory, one compound, NH125, gave results similar to the initial screen in subsequent assays (data not shown). NH125 looked to be an interesting candidate, since it has been shown to be selectively toxic to a wide variety of cancer cell types (97–99) and to sensitize cells to ionizing radiation (100). Moreover, NH125 is a potent inducer of the Integrated Stress Response pathway which bypasses p53-dependent DNA damage pathways (101). However, similar to PD18435, NH125 also showed a preferential inhibition of growth in cells treated with TA alone (data not shown). Therefore, like PD184352, the preferential inhibition of growth in TA/Sh1-treated cells with NH125 is likely due to the ability of TA to sensitize cells to NH125.

Compounds that increase the norm-HI-GFP-sum in response to TA/sh1

Two compounds in the original screen, scriptaid and etomidate, produced nearly a 3-fold increase in the Norm-HI-

Table 2. Fold-change in the Norm-HI-GFP-Sum in response to TA/Sh1 caused by compounds that inhibit C-NHEJ

Compound	Conc (nM)	Day	Fold change ^φ	P-Value*
Scriptaid	1000	6	1.75 ± 0.01	0.007 [§]
Scriptaid	500	6	1.48 ± 0.29	0.064 ^{§ζ}
Scriptaid	1000	5	1.42 ± 0.07	0.003 ^δ
Scriptaid	500	5	1.20 ± 0.07	0.005 ^δ
NU7026	125	5	2.80 ± 0.50	0.055 ^{§ζ}
M3814	1000	5	2.04 ± 0.13	0.004 ^δ
M3814	500	5	2.00 ± 0.12	0.020 ^δ
M3814	250	5	2.14 ± 0.03	<0.001 ^δ
M3814	125	5	2.09 ± 0.10	<0.001 ^δ

*Two-tailed *t*-test *P*-value.^φ± Standard Deviation.[§]Value from follow-up screen, compared with 192 wells treated with TA/Sh1 alone (three plates).^δPerformed in triplicate in the laboratory.^ζNot statistically significant.

GFP-Sum in response to TA/Sh1 compared to the control wells treated with TA/Sh1 alone (top, Figure 4). The results with etomidate were not confirmed in our follow-up screen, however, the results with scriptaid were (Figure 5). At day 6, scriptaid caused a significant 1.75-fold increase in the Norm-HI-GFP-Sum in response to TA/Sh1 at a concentration of 1 μ M (Figure 5B, Table 2). These results with scriptaid were confirmed in the laboratory (Table 2). Scriptaid is an HDAC inhibitor used in cancer therapy (102,103). However, several other HDAC inhibitors in our initial screen did not cause a similar effect (data not shown), suggesting that HDAC was not the target of scriptaid that was responsible for these results.

Neither of the two DNA-PKcs inhibitors in the initial screen, NU7441 and NU7026 (104,105), caused an increase in the Norm-HI-GFP-Sum in response to TA/Sh1 at 1 μ M (data not shown). However, in the follow-up screen, both NU7026 and NU7441 showed a small increase at some concentrations at days 5 and 6, although these increases were not statistically significant (Figure 5, Table 2). This variability in the ability of NU7026 and NU7441 to cause an increase in the Norm-HI-GFP-Sum in response to TA/Sh1 was also observed in experiments done in the laboratory (data not shown). In addition to inhibiting DNA-PKcs, at higher concentrations, NU7026 and NU7441 can also inhibit mTOR (105). We therefore explored the possibility that the variability in the response NU7026 and NU7441 at different concentrations might be due to the inhibition of mTOR, which causes a decrease in the Norm-HI-GFP-Sum in response to TA/Sh1 (Figure 5). To investigate this possibility, a follow-up study was performed in the laboratory with a newer DNA-PKcs inhibitor that does not inhibit mTOR, M3814 (106). Importantly, M3814 caused a 2-fold increase in the Norm-HI-GFP-Sum in response to TA/Sh1 that was significant at all of the concentrations tested, from 125 nM to 1 μ M (Figure 5C, Table 2). These results confirmed that DNA-PKcs is important in preventing telomere loss and CIN resulting from subtelomeric DSBs, and that C-NHEJ is functional in subtelomeric regions.

To further investigate the influence of the various compounds on the repair of DSBs, we analyzed their effect on

the formation of small deletions at an interstitial I-SceI site in cell clone GFP-7F1. As mentioned earlier, this method detects small deletions by the inability of I-SceI to cut a PCR fragment spanning the I-SceI site. Unlike the other compounds tested, both scriptaid and M3814 caused more than a 2-fold increase in the amount of uncut PCR fragment, demonstrating that both compounds caused a large increase in small deletions (Figure 7A, Supplementary Figure S6). The results suggest, that like M3814, scriptaid is an inhibitor of C-NHEJ, consistent with its ability to sensitize cells to ionizing radiation (107). The results also clearly demonstrate that C-NHEJ suppresses the formation of small deletions at I-SceI-induced DSBs, and therefore that small deletions at I-SceI-induced DSBs are formed by Alt-EJ. Small deletions have been shown to be formed by both C-NHEJ and Alt-EJ at blunt-ended Cas9-induced DSBs (108). However, at I-SceI-induced DSBs, which have a 4-nt overhang, the vast majority of repair involving C-NHEJ results in restoration of the I-SceI site (96), which is not the case in cells deficient in C-NHEJ (36,37,109). Thus, the results demonstrate that both C-NHEJ and Alt-EJ help to prevent telomere loss and CIN resulting from subtelomeric DSBs, consistent with a study demonstrating that Alt-EJ is important in preventing chromosome rearrangements (46).

We also used cell clone GFP-7F1 to monitor the effect of various compounds on the frequency of large deletions and/or GCRs at interstitial I-SceI-induced DSBs, as we have previously done with other compounds (17,18,49). With clone GFP-7F1, large deletions and/or GCRs at the I-SceI site are detected by loss of expression of GFP because the I-SceI site is located between the GFP gene and its promoter. Consistent with our earlier results (17,18,49), activation of the inducible I-SceI in clone GFP-7F1 following treatment with TA/Sh1 alone did not result in a significant decrease in GFP-positive cells (Figure 7B) because, unlike at subtelomeric DSBs, large deletions and/or GCRs are very infrequent at interstitial DSBs. However, the addition of M3814, and to a lesser extent scriptaid, caused a large significant increase in large deletions and/or GCRs at the interstitial DSB in response to TA/Sh1 (Figure 7B), as would be expected from the inhibition of C-NHEJ. Thus, the inhibition of C-NHEJ dramatically increases both large and small deletions, indicating that both types of deletions at I-SceI-induced DSBs involve Alt-EJ.

Compounds that did not have a significant effect on the norm-HI-GFP-sum in response to TA/sh1

Some compounds that inhibit ATR and JAK were found to cause a decrease in the Norm-HI-GFP-Sum in response to TA/Sh1 at 1 μ M in the original screen (data not shown). Similarly, the ATR inhibitors AZ20, ETP-46464, VE-821 and VE-822, and the JAK inhibitor TG101348, also caused a large decrease at 1 μ M in the follow-up screen (Figure 5). However, with all of these inhibitors, the dose of 1 μ M significantly inhibited cell growth, whereas at lower concentrations where little effect on cell growth was observed, the decrease in the Norm-HI-GFP-Sum in response to TA/Sh1 was greatly reduced (Supplementary Figure S5). Therefore, although the compounds inhibiting ATR and

JAK may have a modest ability to decrease the Norm-HI-GFP-Sum in response to TA/Sh1, due to their effect on cell growth, the results are inconclusive.

Two other compounds that appeared to cause a decrease in the Norm-HI-GFP-Sum in response to TA/Sh1 in the initial screen, cytidine and aminophylline (data not shown), did not show a similar effect in the follow-up screen (Figure 5). Similarly, three compounds that appeared to cause a moderate increase in the Norm-HI-GFP-Sum in response to TA/Sh1 in the initial screen, sirtinol, EX-527, and betalaphachone (data not shown), did not have an effect in the follow up screen (Figure 5).

In addition to the compounds mentioned above, a variety of other compounds were included in the curated follow-up screen. Two ATM inhibitors, KU-55933 and KU-60019 (110), were included because ATM is an important signaling protein in the DDR (29,111). KU-55933 at 10 μ M was previously reported by us to influence the outcome of I-SceI-induced DSBs at both interstitial and subtelomeric sites (18). However, in our current studies, KU-55933 and KU-60019 had little or no effect on the Norm-HI-GFP-Sum in response to TA/Sh1, either in the initial screen at 1 μ M (data not shown) or the follow-up screen at any of the concentrations tested (Figure 5). These results are consistent with other studies that even the highest concentration used in our current screens, 1 μ M, is not sufficient to generate a response with either KU-55933 (112) or KU-60019 (113,114).

DISCUSSION

Proteins affecting the sensitivity of subtelomeric regions to DSBs

The results presented here provide new insights into the mechanism responsible for the sensitivity of subtelomeric regions to DSBs, and in doing so provide insights into the mechanisms of generation of DSB-induced mutations. The sensitivity of subtelomeric regions to DSBs is characterized by a high frequency of large deletions and GCRs, which has been observed in yeast (115), mouse embryonic stem cells (20), and human cancer cells (16–19,49). Although telomeric repeat sequences are also sensitive to DSBs, there are important differences in the sensitivity of subtelomeric regions and telomeric repeat sequences to DSBs. DSBs within telomeric repeat sequences are not repaired by C-NHEJ (48,116,117). Instead, enzymatically-induced DSBs in telomeric repeat sequences in dividing human cells have been reported to be repaired by either HDR (116), or a combination of Alt-EJ and HDR (48). To explain these results, it was proposed that enzymatically-induced DSBs may be generated during S phase when resection is involved in DSB repair (48). However, as we have previously reported (117), enzymatically-induced DSBs in telomeric repeat sequences in cells in G1 are also resected but not repaired, and therefore resection in telomeric repeat sequences is not dependent on cells being in S/G2 at the time that I-SceI-induced DSBs occur. As a result, it was proposed that the resection at DSBs in telomeric repeat sequences may be the result of a failed attempt to generate the single-stranded overhang required to re-establish a t-loop to protect the end of the chromosome (117).

Unlike with telomeric repeat sequences, our current results demonstrate that subtelomeric DSBs are efficiently repaired by C-NHEJ, as shown by the fact that inhibition of DNA-PKcs has a dramatic effect on the frequency of both large (Figure 5) and small (Figure 7A, Supplementary Figure S6) deletions. Therefore, as we have previously proposed (49), our results suggest that the sensitivity of subtelomeric regions to DSBs being a result of inappropriate resection, which indirectly inhibits DSB repair by C-NHEJ. This inappropriate resection of DSBs at subtelomeric DSBs is consistent with our observation that not only are large deletions more frequent at subtelomeric DSBs, they are also much greater in size (19). Inappropriate resection is also consistent with the increased frequency of GCRs observed at subtelomeric DSBs (17), which may or may not occur in conjunction with large deletions (16). These GCRs appear to involve Alt-EJ, as indicated by the presence of microhomology at the recombination junctions (20), and results demonstrating that Alt-EJ can occur with or without extensive resection (45,118,119).

The effect of compounds on the frequency of small deletions provides important information on the mechanisms of repair of subtelomeric DSBs. The inhibition of DNA-PKcs greatly increased the frequency of small deletions (Figure 7A, Supplementary Figure S6), which unlike large deletions, occur at the same frequency at interstitial and subtelomeric DSBs (17,18,49). The increase in small deletions in response to inhibition of DNA-PKcs demonstrates that small deletions at I-SceI-induced DSBs are formed by Alt-EJ. Therefore, like C-NHEJ, Alt-EJ has an important role in preventing telomere loss due to DSBs in subtelomeric regions. Although C-NHEJ can cause small deletions (108,120), with I-SceI-induced DSBs, C-NHEJ almost always results in restoration of the I-SceI site (36), which does not occur in Ku-deficient cells (36,37,109). It was previously thought that Alt-EJ was primarily involved in the formation of large deletions and GCRs in cells that were defective in C-NHEJ (121). However, it is now clear that Alt-EJ mediated by Pol θ rejoins DSBs in cells without defects in C-NHEJ (108) and is important in maintaining chromosome stability (46). Alt-EJ mediated by Pol θ is involved in the formation of small deletions utilizing 3 bp of microhomology or more (45,108,122–124), which must be located within 15 base pairs on either side of the DSB (122), limiting these deletions to less than 30 base pairs.

The compounds identified in our screen that decrease the Norm-HI-GFP-Sum in response to TA/Sh1 provide clues as to the mechanism responsible for the sensitivity of subtelomeric regions to DSBs. The inhibitors of mTOR, p38 and tankyrase all decreased the Norm-HI-GFP-Sum in response to TA/Sh1 (Figures 4 and 5). mTOR and p38 are important in protecting cells against stress (73,82). Although mTOR and p38 can promote cell death in cells with telomere loss or CIN, this is not the mechanism by which they decrease the Norm-HI-GFP-Sum in response to TA/Sh1, since they did not preferentially inhibit the growth of cells treated with TA/Sh1 (Figure 8). Instead, the inhibitors mTOR and p38 appear to decrease the frequency of telomere loss resulting from subtelomeric DSBs, possibly by inhibiting attempted repair by HDR. The fact that inhibition of p38 prevents DSB-induced telomere loss in

only half of the cells could mean that p38 only promotes telomere loss due to subtelomeric DSBs during a certain part of the cell cycle. Both mTOR (74,75) and p38 (125) promote HDR, which if not completed could lead to large deletions, telomere loss, and GCRs. A role for HDR in the sensitivity of subtelomeric regions to DSBs is consistent with our earlier results demonstrating that there is a much greater amount of BRCA1, RAD51 and CtIP at subtelomeric DSBs compared with interstitial DSBs (55). Other studies have also found that HDR can be deleterious when attempted near telomeres. HDR is involved in the sister chromatid fusions responsible for senescence in normal human cells with shortened telomeres (126,127). Similarly, HDR is involved in the generation of the branched DNA structures and extensive resection resulting in chromosome fusions in POT1-deficient cells (128).

A role for HDR in the sensitivity of subtelomeric regions to DSBs is also consistent with the results presented here demonstrating that both of the compounds in the screen that inhibit tankyrase almost completely eliminated DSB-induced telomere loss. Tankyrase 1 and 2 have been shown to be recruited to I-SceI-induced DSBs, where they stabilized the BRCA1 complex and promote HDR and cell cycle checkpoints (93). Tankyrase 1 also relaxes telomere cohesion after DNA replication to allow for separation of sister chromatid telomeres prior to mitosis (129). A reduced amount of tankyrase 1 at telomeres as a result of shortened telomeres in aged human fibroblasts causes prolonged sister chromatid telomere cohesion that protects against detrimental subtelomeric recombination with other chromosomes (130). Importantly, this subtelomeric recombination resulting from shorter telomere cohesion times due to tankyrase 1 was found to be dependent on ATR and RAD51, suggesting that HDR is involved. Therefore, compounds that inhibit tankyrase may help prevent telomere loss due to subtelomeric DSBs by both preventing HDR and by prolonging G2 to allow for successful repair of the resected DSBs by Alt-EJ.

One possible explanation for why HDR may be deleterious when attempted at subtelomeric DSBs is a deficiency in 53BP1 in subtelomeric regions. 53BP1 regulates the more extensive resection by EXO1 or DNA2/BLM (131–134). Although the loss of 53BP1 overcomes the deficiency in HDR in BRCA1-deficient cells, the HDR in 53BP1-deficient cells is only partially restored (133,135), indicating that some of the more extensively resected ends can no longer be used efficiently in HDR. Consistent with this observation, Pol θ -mediated Alt-EJ is essential in 53BP1-deficient cells (136). 53BP1 also plays a critical role in slow C-NHEJ, where it prevents more extensive resection (137). Therefore, a deficiency in 53BP1 in subtelomeric regions could contribute to excessive resection at subtelomeric DSB, both during HDR in S/G2 and with slow C-NHEJ in G1. A role of 53BP1 in the sensitivity of subtelomeric regions to DSBs is consistent with observations that 53BP1 is dysfunctional in telomeric regions. We have previously shown that although DSBs in telomeric repeat sequences in G1 induce early signatures of the DDR, 53BP1 did not localize to the site of the DSBs (117). A study by Doksani *et al.* (48) also showed that 53BP1 is not involved in repair of DSBs within telomeric repeat sequences, and

that these DSBs also showed extensive resection. In addition, an inability of 53BP1 to prevent resection near telomeres has been observed in *Saccharomyces pombe* (138), in which resection is increased at uncapped telomeres due to decreased recruitment of Rad9, the 53BP1 ortholog. Similarly, in *Saccharomyces cerevisiae*, which shows sensitivity to I-SceI-induced DSBs near telomeres (115), the 53BP1 ortholog, Crb2 also binds less efficiently at uncapped telomeres than at interstitial DSBs (139).

The identification of new compounds for cancer therapy

The results of our screen demonstrate that this assay can be used for the identification of new compounds that inhibit C-NHEJ. Inhibition of C-NHEJ is currently being investigated as a means of sensitizing cancer cells to ionizing radiation or chemotherapy (140–142). The efforts to identify C-NHEJ inhibitors has primarily been focused on DNA-PKcs. However, due to the involvement of DNA-PKcs in a number of different pathways (28), these inhibitors are likely to cause numerous side effects, and therefore may not be optimal as therapeutic agents. An unbiased approach, such as the assay presented here, may therefore provide the means of identifying other druggable targets that may be more suitable for sensitizing cancer cells to ionizing radiation or chemotherapy.

It remains to be determined whether this screen is capable of identifying compounds that target proteins or pathways that selectively eliminate cells experiencing telomere loss and/or CIN. These compounds could be used to selectively target cancer cells, which commonly experience an increased rates of spontaneous telomere loss (8,9) as a result of oncogene-induced replication stress (5). Our previous studies have shown that cancer cells can have widely different rates of telomere instability (143,144). EJ-30, the cancer cell line used in the current study was chosen because it has a relatively low rate of telomere loss, as reflected in its relatively stable genome with 46 chromosomes. Due to this low background of spontaneous telomere loss, following the loss of the telomere on the marker chromosome 16, the CIN in the EJ-30 cancer cell line is primarily confined to that chromosome, as determined by the presence of anaphase bridges involving only chromosome 16 (14). As a result, compounds that selectively target cells that have lost a telomere and/or are experiencing CIN in our assay system should primarily affect cells that have recently undergone the I-SceI-induced telomere loss.

In view of our results, future attempts at identifying compounds that specifically eliminate cells experiencing telomere loss and/or CIN will focus on a variation of the assay. In this modified assay, the mS11fs cells are pre-treated with TA/Sh1 for 3 days prior to plating in the 384-well plates. The test compounds are then added the day after plating, and the percentage of GFP-positive cells is monitored for 6 days, by which time 35% of the control cells will be GFP-positive. Compounds that selectively eliminate cells that have lost a telomere and/or have CIN can then be identified by their ability to cause a decrease the percentage of GFP-positive cells. Importantly, this approach avoids the simultaneous treatment with TA/Sh1 and the test compounds in our current assay, and therefore avoids po-

tential artifacts stemming from the sensitization of cells to compounds by TA, and avoids possible inhibition of growth by the compounds, which inhibits the generation of GFP-positive cells by TA/Sh1. The success of this approach will depend on the continued presence of cells in the population with telomere loss and/or CIN for several days after the initial telomere loss caused by TA/Sh1-induced DSBs. We have previously shown that spontaneous telomere loss in EJ-30 results in sister chromatid fusions that initiate B/F/B cycles that continue for many cell generations (14,15). Although I-SceI-induced telomere loss results in a wide variety of GCRs (19), not all of which are unstable (e.g. translocations), many cells in this assay will also experience prolonged B/F/B cycles that would provide targets for compounds that selectively eliminate cells with telomere loss and/or CIN. Although the success of this approach is uncertain, the importance of identifying compounds that can selectively target cancer cells with telomere loss and/or CIN makes these studies well worth the effort.

DATA AVAILABILITY

The raw and analyzed screening data are available through the UCSF Small Molecule Discovery Center at <https://hits.ucsf.edu/project/show/271>. Requires registration for a free account.

SUPPLEMENTARY DATA

Supplementary Data are available at NAR Cancer Online.

ACKNOWLEDGEMENTS

Douglas Miller provided technical support.
Author contributions: C.W. provided technical advice on high-throughput screens and performed the screen. J.P.M. conceived of the project, constructed the plasmids and cell clone utilized in the project, analyzed the data, and wrote the manuscript.

FUNDING

UCSF Department of Radiation Oncology.
Conflict of interest statement. None declared.

REFERENCES

- McGranahan, N. and Swanton, C. (2015) Biological and therapeutic impact of intratumor heterogeneity in cancer evolution. *Cancer Cell*, **27**, 15–26.
- Bakhom, S.F. and Landau, D.A. (2017) Chromosomal instability as a driver of tumor heterogeneity and evolution. *Cold Spring Harb. Perspect. Med.*, **7**, a029611.
- Kotsantis, P., Petermann, E. and Boulton, S.J. (2018) Mechanisms of oncogene-induced replication stress: Jigsaw falling into place. *Cancer Discov.*, **8**, 537–555.
- Muraki, K., Nyhan, K., Han, L. and Murnane, J.P. (2012) Mechanisms of telomere loss and their consequences for chromosome instability. *Front. Oncol.*, **2**, 135.
- Murnane, J.P. (2010) Telomere loss as a mechanism for chromosome instability in human cancer. *Cancer Res.*, **70**, 4255–4259.
- Blackburn, E.H., Epel, E.S. and Lin, J. (2015) Human telomere biology: a contributory and interactive factor in aging, disease risks, and protection. *Science*, **350**, 1193–1198.
- de Lange, T. (2018) Shelterin-mediated telomere protection. *Annu. Rev. Genet.*, **52**, 223–247.
- Gisselsson, D., Gorunova, L., Hoglund, M., Mandahl, N. and Elfving, P. (2004) Telomere shortening and mitotic dysfunction generate cytogenetic heterogeneity in a subgroup of renal cell carcinomas. *Br. J. Cancer*, **91**, 327–332.
- Gisselsson, D., Jonson, T., Petersen, A., Strombeck, B., Dal Cin, P., Hoglund, M., Mitelman, F., Mertens, F. and Mandahl, N. (2001) Telomere dysfunction triggers extensive DNA fragmentation and evolution of complex chromosome abnormalities in human malignant tumors. *Proc. Natl. Acad. Sci. U.S.A.*, **98**, 12683–12688.
- Huda, N., Xu, Y., Bates, A.M., Rankin, D.A., Kannan, N. and Gilley, D. (2019) Onset of telomere dysfunction and fusions in human ovarian carcinoma. *Cells*, **8**, 414.
- Tu, L., Huda, N., Grimes, B.R., Slee, R.B., Bates, A.M., Cheng, L. and Gilley, D. (2016) Widespread telomere instability in prostatic lesions. *Mol. Carcinog.*, **55**, 842–852.
- O'Toole, C.M., Povey, S., Hepburn, P. and Franks, L.M. (1983) Identity of some human bladder cancer cell lines. *Nature*, **301**, 429–430.
- Fouladi, B., Sabatier, L., Miller, D., Pottier, G. and Murnane, J.P. (2000) The relationship between spontaneous telomere loss and chromosome instability in a human tumor cell line. *Neoplasia*, **2**, 540–554.
- Lo, A.W., Sabatier, L., Fouladi, B., Pottier, G., Ricoul, M. and Murnane, J.P. (2002) DNA amplification by breakage/fusion/bridge cycles initiated by spontaneous telomere loss in a human cancer cell line. *Neoplasia*, **4**, 531–538.
- Sabatier, L., Ricoul, M., Pottier, G. and Murnane, J.P. (2005) The loss of a single telomere can result in instability of multiple chromosomes in a human tumor cell line. *Mol. Cancer Res.*, **3**, 139–150.
- Kulkarni, A., Zschenker, O., Reynolds, G., Miller, D. and Murnane, J.P. (2010) Effect of telomere proximity on telomere position effect, chromosome healing, and sensitivity to DNA double-strand breaks in a human tumor cell line. *Mol. Cell. Biol.*, **30**, 578–589.
- Miller, D., Reynolds, G.E., Mejia, R., Stark, J.M. and Murnane, J.P. (2011) Subtelomeric regions in mammalian cells are deficient in DNA double-strand break repair. *DNA Repair (Amst.)*, **10**, 536–544.
- Muraki, K., Han, L., Miller, D. and Murnane, J.P. (2013) The role of ATM in the deficiency in nonhomologous end-joining near telomeres in a human cancer cell line. *PLoS Genet.*, **9**, e1003386.
- Zschenker, O., Kulkarni, A., Miller, D., Reynolds, G.E., Granger-Locatelli, M., Pottier, G., Sabatier, L. and Murnane, J.P. (2009) Increased sensitivity of subtelomeric regions to DNA double-strand breaks in a human cancer cell line. *DNA Repair (Amst.)*, **8**, 886–900.
- Lo, A.W., Sprung, C.N., Fouladi, B., Pedram, M., Sabatier, L., Ricoul, M., Reynolds, G.E. and Murnane, J.P. (2002) Chromosome instability as a result of double-strand breaks near telomeres in mouse embryonic stem cells. *Mol. Cell. Biol.*, **22**, 4836–4850.
- Fumagalli, M., Rossiello, F., Clerici, M., Barozzi, S., Cittaro, D., Kaplunov, J.M., Bucci, G., Dobrev, M., Matti, V., Beausejour, C.M. et al. (2012) Telomeric DNA damage is irreparable and causes persistent DNA-damage-response activation. *Nat. Cell Biol.*, **14**, 355–365.
- Hewitt, G., Jurk, D., Marques, F.D., Correia-Melo, C., Hardy, T., Gackowska, A., Anderson, R., Taschuk, M., Mann, J. and Passos, J.F. (2012) Telomeres are favoured targets of a persistent DNA damage response in ageing and stress-induced senescence. *Nat. Commun.*, **3**, 708.
- Ackerson, S.M., Romney, C., Schuck, P.L. and Stewart, J.A. (2021) To join or not to join: decision points along the pathway to double-strand break repair vs. chromosome end protection. *Front. Cell Dev. Biol.*, **9**, 708763.
- Scully, R., Panday, A., Elango, R. and Willis, N.A. (2019) DNA double-strand break repair-pathway choice in somatic mammalian cells. *Nat. Rev. Mol. Cell Biol.*, **20**, 698–714.
- Deshpande, R.A., Myler, L.R., Soniat, M.M., Makharashvili, N., Lee, L., Lees-Miller, S.P., Finkelstein, I.J. and Paull, T.T. (2020) DNA-dependent protein kinase promotes DNA end processing by MRN and CtIP. *Sci. Adv.*, **6**, eaay0922.

26. Langerak,P., Mejia-Ramirez,E., Limbo,O. and Russell,P. (2011) Release of Ku and MRN from DNA ends by Mre11 nuclease activity and Ctp1 is required for homologous recombination repair of double-strand breaks. *PLoS Genet.*, **7**, e1002271.
27. Jette,N. and Lees-Miller,S.P. (2015) The DNA-dependent protein kinase: a multifunctional protein kinase with roles in DNA double strand break repair and mitosis. *Prog Biophys. Mol. Biol.*, **117**, 194–205.
28. Yue,X., Bai,C., Xie,D., Ma,T. and Zhou,P.K. (2020) DNA-PKcs: a multi-faceted player in DNA damage response. *Front Genet*, **11**, 607428.
29. Williams,R.M., Yates,L.A. and Zhang,X. (2020) Structures and regulations of ATM and ATR, master kinases in genome integrity. *Curr. Opin. Struct. Biol.*, **61**, 98–105.
30. Chapman,J.R., Barral,P., Vannier,J.B., Borel,V., Steger,M., Tomas-Loba,A., Sartori,A.A., Adams,I.R., Batista,F.D. and Boulton,S.J. (2013) RIF1 is essential for 53BP1-dependent nonhomologous end joining and suppression of DNA double-strand break resection. *Mol. Cell*, **49**, 858–871.
31. Bakr,A., Oing,C., Kocher,S., Borgmann,K., Dornreiter,I., Petersen,C., Dikomey,E. and Mansour,W.Y. (2015) Involvement of ATM in homologous recombination after end resection and RAD51 nucleofilament formation. *Nucleic Acids Res.*, **43**, 3154–3166.
32. Attwooll,C.L., Akpinar,M. and Petrini,J.H. (2009) The mre11 complex and the response to dysfunctional telomeres. *Mol. Cell Biol.*, **29**, 5540–5551.
33. Deng,Y., Guo,X., Ferguson,D.O. and Chang,S. (2009) Multiple roles for MRE11 at uncapped telomeres. *Nature*, **460**, 914–918.
34. Dimitrova,N. and de Lange,T. (2009) Cell cycle-dependent role of MRN at dysfunctional telomeres: ATM signaling-dependent induction of nonhomologous end joining (NHEJ) in G1 and resection-mediated inhibition of NHEJ in G2. *Mol. Cell Biol.*, **29**, 5552–5563.
35. Helmink,B.A., Tubbs,A.T., Dorsett,Y., Bednarski,J.J., Walker,L.M., Feng,Z., Sharma,G.G., McKinnon,P.J., Zhang,J., Bassing,C.H. *et al.* (2011) H2AX prevents CtIP-mediated DNA end resection and aberrant repair in G1-phase lymphocytes. *Nature*, **469**, 245–249.
36. Bennardo,N., Cheng,A., Huang,N. and Stark,J.M. (2008) Alternative-NHEJ is a mechanistically distinct pathway of mammalian chromosome break repair. *PLoS Genet.*, **4**, e1000110.
37. Guirouilh-Barbat,J., Huck,S., Bertrand,P., Pizio,L., Desmaze,C., Sabatier,L. and Lopez,B.S. (2004) Impact of the KU80 pathway on NHEJ-induced genome rearrangements in mammalian cells. *Mol. Cell*, **14**, 611–623.
38. Rass,E., Grabarz,A., Plo,I., Gautier,J., Bertrand,P. and Lopez,B.S. (2009) Role of Mre11 in chromosomal nonhomologous end joining in mammalian cells. *Nat. Struct. Mol. Biol.*, **16**, 819–824.
39. Xie,A., Kwok,A. and Scully,R. (2009) Role of mammalian Mre11 in classical and alternative nonhomologous end joining. *Nat. Struct. Mol. Biol.*, **16**, 814–818.
40. Yan,C.T., Boboila,C., Souza,E.K., Franco,S., Hickernell,T.R., Murphy,M., Gumaste,S., Geyer,M., Zarrin,A.A., Manis,J.P. *et al.* (2007) IgH class switching and translocations use a robust non-classical end-joining pathway. *Nature*, **449**, 478–482.
41. Guirouilh-Barbat,J., Rass,E., Plo,I., Bertrand,P. and Lopez,B.S. (2007) Defects in XRCC4 and KU80 differentially affect the joining of distal nonhomologous ends. *Proc. Natl. Acad. Sci. U.S.A.*, **104**, 20902–20907.
42. Weinstock,D.M., Brunet,E. and Jasin,M. (2007) Formation of NHEJ-derived reciprocal chromosomal translocations does not require Ku70. *Nat. Cell Biol.*, **9**, 978–981.
43. Zhang,Y. and Jasin,M. (2011) An essential role for CtIP in chromosomal translocation formation through an alternative end-joining pathway. *Nat. Struct. Mol. Biol.*, **18**, 80–84.
44. Ramsden,D.A., Carvajal-Garcia,J. and Gupta,G.P. (2022) Mechanism, cellular functions and cancer roles of polymerase-theta-mediated DNA end joining. *Nat. Rev. Mol. Cell Biol.*, **23**, 125–140.
45. Wyatt,D.W., Feng,W., Conlin,M.P., Yousefzadeh,M.J., Roberts,S.A., Mieczkowski,P., Wood,R.D., Gupta,G.P. and Ramsden,D.A. (2016) Essential roles for polymerase theta-mediated end joining in the repair of chromosome breaks. *Mol. Cell*, **63**, 662–673.
46. Yousefzadeh,M.J., Wyatt,D.W., Takata,K., Mu,Y., Hensley,S.C., Tomida,J., Bylund,G.O., Double,S., Johansson,E., Ramsden,D.A. *et al.* (2014) Mechanism of suppression of chromosomal instability by DNA polymerase POLQ. *PLoS Genet.*, **10**, e1004654.
47. Karlseder,J., Hoke,K., Mirzoeva,O.K., Bakkenist,C., Kastan,M.B., Petrini,J.H. and de Lange,T. (2004) The telomeric protein TRF2 binds the ATM kinase and can inhibit the ATM-dependent DNA damage response. *PLoS Biol.*, **2**, E240.
48. Doksani,Y. and de Lange,T. (2016) Telomere-internal double-strand breaks are repaired by homologous recombination and PARP1/Lig3-dependent end-joining. *Cell Rep.*, **17**, 1646–1656.
49. Muraki,K., Han,L., Miller,D. and Murnane,J.P. (2015) Processing by MRE11 is involved in the sensitivity of subtelomeric regions to DNA double-strand breaks. *Nucleic Acids Res.*, **43**, 7911–7930.
50. Stegmeier,F., Hu,G., Rickles,R.J., Hannon,G.J. and Elledge,S.J. (2005) A lentiviral microRNA-based system for single-copy polymerase II-regulated RNA interference in mammalian cells. *Proc. Natl. Acad. Sci. U.S.A.*, **102**, 13212–13217.
51. Rechsteiner,M. (1990) PEST sequences are signals for rapid intracellular proteolysis. *Semin. Cell Biol.*, **1**, 433–440.
52. Hanish,J.P., Yanowitz,J.L. and de Lange,T. (1994) Stringent sequence requirements for the formation of human telomeres. *Proc. Natl. Acad. Sci. U.S.A.*, **91**, 8861–8865.
53. Bindra,R.S., Goglia,A.G., Jasin,M. and Powell,S.N. (2013) Development of an assay to measure mutagenic non-homologous end-joining repair activity in mammalian cells. *Nucleic Acids Res.*, **41**, e115.
54. Bindels,D.S., Haarbosch,L., van Weeren,L., Postma,M., Wiese,K.E., Mastop,M., Aumonier,S., Gotthard,G., Royant,A., Hink,M.A. *et al.* (2017) mScarlet: a bright monomeric red fluorescent protein for cellular imaging. *Nat. Methods*, **14**, 53–56.
55. Silva,Alcaraz, Jones,B. and Murnane,J.P. (2017) Differences in the recruitment of DNA repair proteins at subtelomeric and interstitial I-SceI endonuclease-induced DNA double-strand breaks. *DNA Repair (Amst.)*, **49**, 1–8.
56. Honma,M., Sakuraba,M., Koizumi,T., Takashima,Y., Sakamoto,H. and Hayashi,M. (2007) Non-homologous end-joining for repairing I-SceI-induced DNA double strand breaks in human cells. *DNA Repair (Amst.)*, **6**, 781–788.
57. Rebuzzini,P., Khorrauli,L., Azzalin,C.M., Magnani,E., Mondello,C. and Giulotto,E. (2005) New mammalian cellular systems to study mutations introduced at the break site by non-homologous end-joining. *DNA Repair (Amst.)*, **4**, 546–555.
58. Sargent,R.G., Brenneman,M.A. and Wilson,J.H. (1997) Repair of site-specific double-strand breaks in a mammalian chromosome by homologous and illegitimate recombination. *Mol. Cell Biol.*, **17**, 267–277.
59. Varga,T. and Aplan,P.D. (2005) Chromosomal aberrations induced by double strand DNA breaks. *DNA Repair (Amst.)*, **4**, 1038–1046.
60. Gossen,M. and Bujard,H. (1992) Tight control of gene expression in mammalian cells by tetracycline-responsive promoters. *Proc. Natl. Acad. Sci. U.S.A.*, **89**, 5547–5551.
61. Laberthonniere,C., Magdinier,F. and Robin,J.D. (2019) Bring It to an end: does telomeres size matter? *Cells*, **8**, 30.
62. Gao,Q., Reynolds,G.E., Innes,L., Pedram,M., Jones,E., Junabi,M., Gao,D.W., Ricoul,M., Sabatier,L., Van Brocklin,H. *et al.* (2007) Telomeric transgenes are silenced in adult mouse tissues and embryo fibroblasts but are expressed in embryonic stem cells. *Stem Cells*, **25**, 3085–3092.
63. Hsu,Y.L., Kuo,P.L., Lin,L.T. and Lin,C.C. (2005) Asiatic acid, a triterpene, induces apoptosis and cell cycle arrest through activation of extracellular signal-regulated kinase and p38 mitogen-activated protein kinase pathways in human breast cancer cells. *J. Pharmacol. Exp. Ther.*, **313**, 333–344.
64. Casas-Selves,M., Kim,J., Zhang,Z., Helfrich,B.A., Gao,D., Porter,C.C., Scarborough,H.A., Bunn,P.A., Chan,D.C., Tan,A.C. *et al.* (2012) Tankyrase and the canonical Wnt pathway protect lung cancer cells from EGFR inhibition. *Cancer Res.*, **72**, 4154–4164.
65. Huang,S.M., Mishina,Y.M., Liu,S., Cheung,A., Stegmeier,F., Michaud,G.A., Charlat,O., Willelte,E., Zhang,Y., Wiessner,S. *et al.* (2009) Tankyrase inhibition stabilizes axin and antagonizes Wnt signalling. *Nature*, **461**, 614–620.
66. Narwal,M., Koivunen,J., Haikarainen,T., Obaji,E., Legala,O.E., Venkannagari,H., Joensuu,P., Pihlajaniemi,T. and Lehtio,L. (2013) Discovery of tankyrase inhibiting flavones with increased potency and isoenzyme selectivity. *J. Med. Chem.*, **56**, 7880–7889.

67. Eyre, T.A., Collins, G.P., Goldstone, A.H. and Cwynarski, K. (2014) Time now to TORC the TORC? New developments in mTOR pathway inhibition in lymphoid malignancies. *Br. J. Haematol.*, **166**, 336–351.
68. Falcon, B.L., Barr, S., Gokhale, P.C., Chou, J., Fogarty, J., Depeille, P., Miglarese, M., Epstein, D.M. and McDonald, D.M. (2011) Reduced VEGF production, angiogenesis, and vascular regrowth contribute to the antitumor properties of dual mTORC1/mTORC2 inhibitors. *Cancer Res.*, **71**, 1573–1583.
69. Pei, Z., Blackwood, E., Liu, L., Malek, S., Belvin, M., Koehler, M.F., Ortwein, D.F., Chen, H., Cohen, F., Kenny, J.R. *et al.* (2013) Discovery and biological profiling of potent and selective mTOR inhibitor GDC-0349. *ACS Med. Chem. Lett.*, **4**, 103–107.
70. Shultz, M.D., Cheung, A.K., Kirby, C.A., Firestone, B., Fan, J., Chen, C.H., Chen, Z., Chin, D.N., Dipietro, L., Fazal, A. *et al.* (2013) Identification of NVP-TNKS656: the use of structure-efficiency relationships to generate a highly potent, selective, and orally active tankyrase inhibitor. *J. Med. Chem.*, **56**, 6495–6511.
71. Xing, L., Shieh, H.S., Selness, S.R., Devraj, R.V., Walker, J.K., Devadas, B., Hope, H.R., Compton, R.P., Schindler, J.F., Hirsch, J.L. *et al.* (2009) Structural bioinformatics-based prediction of exceptional selectivity of p38 MAP kinase inhibitor PH-797804. *Biochemistry*, **48**, 6402–6411.
72. Guichard, S.M., Curwen, J., Bihani, T., D’Cruz, C.M., Yates, J.W., Grondine, M., Howard, Z., Davies, B.R., Bigley, G., Klinowska, T. *et al.* (2015) AZD2014, an inhibitor of mTORC1 and mTORC2, is highly effective in ER+ breast cancer when administered using intermittent or continuous schedules. *Mol. Cancer Ther.*, **14**, 2508–2518.
73. Populo, H., Lopes, J.M. and Soares, P. (2012) The mTOR signalling pathway in human cancer. *Int. J. Mol. Sci.*, **13**, 1886–1918.
74. Ma, Y., Vassetzky, Y. and Dokudovskaya, S. (2018) mTORC1 pathway in DNA damage response. *Biochim. Biophys. Acta Mol. Cell. Res.*, **1865**, 1293–1311.
75. El Botty, R., Coussy, F., Hatem, R., Assayag, F., Chateau-Joubert, S., Servely, J.L., Leboucher, S., Fouillade, C., Vacher, S., Ouine, B. *et al.* (2018) Inhibition of mTOR downregulates expression of DNA repair proteins and is highly efficient against BRCA2-mutated breast cancer in combination to PARP inhibition. *Oncotarget*, **9**, 29587–29600.
76. Kaieda, A., Takahashi, M., Takai, T., Goto, M., Miyazaki, T., Hori, Y., Unno, S., Kawamoto, T., Tanaka, T., Itono, S. *et al.* (2018) Structure-based design, synthesis, and biological evaluation of imidazo[1,2-b]pyridazine-based p38 MAP kinase inhibitors. *Bioorg. Med. Chem.*, **26**, 647–660.
77. Patnaik, A., Haluska, P., Tolcher, A.W., Erlichman, C., Papadopoulos, K.P., Lensing, J.L., Beeram, M., Molina, J.R., Rasco, D.W., Arcos, R.R. *et al.* (2016) A first-in-human phase I study of the Oral p38 MAPK inhibitor, Ralimetinib (LY2228820 Dimesylate), in patients with advanced cancer. *Clin. Cancer Res.*, **22**, 1095–1102.
78. Ishitsuka, K., Hideshima, T., Neri, P., Vallet, S., Shiraiishi, N., Okawa, Y., Shen, Z., Raje, N., Kiziltepe, T., Ocio, E.M. *et al.* (2008) p38 mitogen-activated protein kinase inhibitor LY2228820 enhances bortezomib-induced cytotoxicity and inhibits osteoclastogenesis in multiple myeloma; therapeutic implications. *Br. J. Haematol.*, **141**, 598–606.
79. Mader, M., de Dios, A., Shih, C., Bonjouklian, R., Li, T., White, W., Lopez de Uralde, B., Sanchez-Martinez, C., del Prado, M., Jaramillo, C. *et al.* (2008) Imidazolyl benzimidazoles and imidazo[4,5-b]pyridines as potent p38 α MAP kinase inhibitors with excellent in vivo antiinflammatory properties. *Bioorg. Med. Chem. Lett.*, **18**, 179–183.
80. Pargellis, C., Tong, L., Churchill, L., Cirillo, P.F., Gilmore, T., Graham, A.G., Grob, P.M., Hickey, E.R., Moss, N., Pav, S. *et al.* (2002) Inhibition of p38 MAP kinase by utilizing a novel allosteric binding site. *Nat. Struct. Biol.*, **9**, 268–272.
81. Yasui, H., Hideshima, T., Ikeda, H., Jin, J., Ocio, E.M., Kiziltepe, T., Okawa, Y., Vallet, S., Podar, K., Ishitsuka, K. *et al.* (2007) BIRB 796 enhances cytotoxicity triggered by bortezomib, heat shock protein (Hsp) 90 inhibitor, and dexamethasone via inhibition of p38 mitogen-activated protein kinase/Hsp27 pathway in multiple myeloma cell lines and inhibits paracrine tumour growth. *Br. J. Haematol.*, **136**, 414–423.
82. Roy, S., Roy, S., Rana, A., Akhter, Y., Hande, M.P. and Banerjee, B. (2018) The role of p38 MAPK pathway in p53 compromised state and telomere mediated DNA damage response. *Mutat. Res. Genet. Toxicol. Environ. Mutagen.*, **836**, 89–97.
83. Daud, A.I., Krishnamurthi, S.S., Saleh, M.N., Gitlitz, B.J., Borad, M.J., Gold, P.J., Chiorean, E.G., Springett, G.M., Abbas, R., Agarwal, S. *et al.* (2012) Phase I study of bosutinib, a src/abl tyrosine kinase inhibitor, administered to patients with advanced solid tumors. *Clin. Cancer Res.*, **18**, 1092–1100.
84. Hennequin, L.F., Allen, J., Breed, J., Curwen, J., Fennell, M., Green, T.P., Lambert-van der Brempt, C., Morgentin, R., Norman, R.A., Olivier, A. *et al.* (2006) N-(5-chloro-1,3-benzodioxol-4-yl)-7-[2-(4-methylpiperazin-1-yl)ethoxy]-5-(tetrahydro-2H-pyran-4-yloxy)quinazolin-4-amine, a novel, highly selective, orally available, dual-specific c-Src/Abl kinase inhibitor. *J. Med. Chem.*, **49**, 6465–6488.
85. Chang, Y.M., Bai, L., Liu, S., Yang, J.C., Kung, H.J. and Evans, C.P. (2008) Src family kinase oncogenic potential and pathways in prostate cancer as revealed by AZD0530. *Oncogene*, **27**, 6365–6375.
86. Green, T.P., Fennell, M., Whittaker, R., Curwen, J., Jacobs, V., Allen, J., Logie, A., Hargreaves, J., Hickinson, D.M., Wilkinson, R.W. *et al.* (2009) Preclinical anticancer activity of the potent, oral Src inhibitor AZD0530. *Mol. Oncol.*, **3**, 248–261.
87. Khazak, V., Astsaturov, I., Serebriiskii, I.G. and Golemis, E.A. (2007) Selective Raf inhibition in cancer therapy. *Expert Opin. Ther. Targets*, **11**, 1587–1609.
88. Chao, T.S., Abe, M., Hershenson, M.B., Gomes, I. and Rosner, M.R. (1997) Src tyrosine kinase mediates stimulation of Raf-1 and mitogen-activated protein kinase by the tumor promoter thapsigargin. *Cancer Res.*, **57**, 3168–3173.
89. Stokoe, D. and McCormick, F. (1997) Activation of c-Raf-1 by Ras and Src through different mechanisms: activation in vivo and in vitro. *EMBO J.*, **16**, 2384–2396.
90. Lu, J., Ma, Z., Hsieh, J.C., Fan, C.W., Chen, B., Longgood, J.C., Williams, N.S., Amatruda, J.F., Lum, L. and Chen, C. (2009) Structure-activity relationship studies of small-molecule inhibitors of Wnt response. *Bioorg. Med. Chem. Lett.*, **19**, 3825–3827.
91. Dregalla, R.C., Zhou, J., Idate, R.R., Battaglia, C.L., Liber, H.L. and Bailey, S.M. (2010) Regulatory roles of tankyrase 1 at telomeres and in DNA repair: suppression of T-SCE and stabilization of DNA-PKcs. *Aging (Albany NY)*, **2**, 691–708.
92. Kim, M.K. (2018) Novel insight into the function of tankyrase. *Oncol. Lett.*, **16**, 6895–6902.
93. Nagy, Z., Kalousi, A., Furst, A., Koch, M., Fischer, B. and Soutoglou, E. (2016) Tankyrases promote homologous recombination and check point activation in response to DSBs. *PLoS Genet.*, **12**, e1005791.
94. Tripathi, E. and Smith, S. (2017) Cell cycle-regulated ubiquitination of tankyrase 1 by RNF8 and ABRO1/BRCC36 controls the timing of sister telomere resolution. *EMBO J.*, **36**, 503–519.
95. Hsiao, S.J. and Smith, S. (2008) Tankyrase function at telomeres, spindle poles, and beyond. *Biochimie*, **90**, 83–92.
96. Lin, W.Y., Wilson, J.H. and Lin, Y. (2013) Repair of chromosomal double-strand breaks by precise ligation in human cells. *DNA Repair (Amst.)*, **12**, 480–487.
97. Arora, S., Yang, J.M., Kinzy, T.G., Utsumi, R., Okamoto, T., Kitayama, T., Ortiz, P.A. and Hait, W.N. (2003) Identification and characterization of an inhibitor of eukaryotic elongation factor 2 kinase against human cancer cell lines. *Cancer Res.*, **63**, 6894–6899.
98. Arora, S., Yang, J.M., Utsumi, R., Okamoto, T., Kitayama, T. and Hait, W.N. (2004) P-glycoprotein mediates resistance to histidine kinase inhibitors. *Mol. Pharmacol.*, **66**, 460–467.
99. Chen, Z., Gopalakrishnan, S.M., Bui, M.H., Soni, N.B., Warrior, U., Johnson, E.F., Donnelly, J.B. and Glaser, K.B. (2011) 1-Benzyl-3-cetyl-2-methylimidazolium iodide (NH125) induces phosphorylation of eukaryotic elongation factor-2 (eEF2): a cautionary note on the anticancer mechanism of an eEF2 kinase inhibitor. *J. Biol. Chem.*, **286**, 43951–43958.
100. Zhu, H., Song, H., Chen, G., Yang, X., Liu, J., Ge, Y., Lu, J., Qin, Q., Zhang, C., Xu, L. *et al.* (2017) eEF2K Promotes progression and radioresistance of esophageal squamous cell carcinoma. *Radiother. Oncol.*, **124**, 439–447.
101. Sheikh, S., Saxena, D., Tian, X., Amirshaghghi, A., Tsourkas, A., Brem, S. and Dorsey, J.F. (2019) An integrated stress response agent

- that modulates DR5-dependent TRAIL synergy reduces patient-derived glioma stem cell viability. *Mol. Cancer Res.*, **17**, 1102–1114.
102. Damaskos, C., Tomos, I., Garmpis, N., Karakatsani, A., Dimitroulis, D., Garmpi, A., Spartalis, E., Kampolis, C.F., Tsagkari, E., Loukeri, A.A. *et al.* (2018) Histone deacetylase inhibitors as a novel targeted therapy against non-small cell lung cancer: where are we now and what should we expect? *Anticancer Res.*, **38**, 37–43.
 103. Su, G.H., Sohn, T.A., Ryu, B. and Kern, S.E. (2000) A novel histone deacetylase inhibitor identified by high-throughput transcriptional screening of a compound library. *Cancer Res.*, **60**, 3137–3142.
 104. Leahy, J.J., Golding, B.T., Griffin, R.J., Hardcastle, I.R., Richardson, C., Rigoreau, L. and Smith, G.C. (2004) Identification of a highly potent and selective DNA-dependent protein kinase (DNA-PK) inhibitor (NU7441) by screening of chromenone libraries. *Bioorg. Med. Chem. Lett.*, **14**, 6083–6087.
 105. Veuger, S.J., Curtin, N.J., Richardson, C.J., Smith, G.C. and Durkacz, B.W. (2003) Radiosensitization and DNA repair inhibition by the combined use of novel inhibitors of DNA-dependent protein kinase and poly(ADP-ribose) polymerase-1. *Cancer Res.*, **63**, 6008–6015.
 106. Zenke, F.T., Zimmermann, A., Sirrenberg, C., Dahmen, H., Kirkin, V., Pehl, U., Grombacher, T., Wilm, C., Fuchss, T., Amendt, C. *et al.* (2020) Pharmacologic inhibitor of DNA-PK, M3814, potentiates radiotherapy and regresses human tumors in mouse models. *Mol. Cancer Ther.*, **19**, 1091–1101.
 107. Kuribayashi, T., Ohara, M., Sora, S. and Kubota, N. (2010) Scriptaid, a novel histone deacetylase inhibitor, enhances the response of human tumor cells to radiation. *Int. J. Mol. Med.*, **25**, 25–29.
 108. Hussain, S.S., Majumdar, R., Moore, G.M., Narang, H., Buechelmaier, E.S., Bazil, M.J., Ravindran, P.T., Leeman, J.E., Li, Y., Jalan, M. *et al.* (2021) Measuring nonhomologous end-joining, homologous recombination and alternative end-joining simultaneously at an endogenous locus in any transfectable human cell. *Nucleic Acids Res.*, **49**, e74.
 109. Ma, J.L., Kim, E.M., Haber, J.E. and Lee, S.E. (2003) Yeast Mre11 and Rad1 proteins define a Ku-independent mechanism to repair double-strand breaks lacking overlapping end sequences. *Mol. Cell Biol.*, **23**, 8820–8828.
 110. Golding, S.E., Rosenberg, E., Valerie, N., Hussaini, I., Frigerio, M., Cockcroft, X.F., Chong, W.Y., Hummerson, M., Rigoreau, L., Menear, K.A. *et al.* (2009) Improved ATM kinase inhibitor KU-60019 radiosensitizes glioma cells, compromises insulin, AKT and ERK prosurvival signaling, and inhibits migration and invasion. *Mol. Cancer Ther.*, **8**, 2894–2902.
 111. Shiloh, Y. (2014) ATM: expanding roles as a chief guardian of genome stability. *Exp. Cell Res.*, **329**, 154–161.
 112. Bryant, H.E. and Helleday, T. (2006) Inhibition of poly (ADP-ribose) polymerase activates ATM which is required for subsequent homologous recombination repair. *Nucleic Acids Res.*, **34**, 1685–1691.
 113. Bermudez-Cabrera, H.C., Culbertson, S., Barkal, S., Holmes, B., Shen, M.W., Zhang, S., Gifford, D.K. and Sherwood, R.I. (2021) Small molecule inhibition of ATM kinase increases CRISPR-Cas9 1-bp insertion frequency. *Nat. Commun.*, **12**, 5111.
 114. Scotto, L., Serrano, X.J., Zullo, K., Kinahan, C., Deng, C., Sawas, A., Bates, S. and O'Connor, O.A. (2020) ATM inhibition overcomes resistance to histone deacetylase inhibitor due to p21 induction and cell cycle arrest. *Oncotarget*, **11**, 3432–3442.
 115. Ricchetti, M., Dujon, B. and Fairhead, C. (2003) Distance from the chromosome end determines the efficiency of double strand break repair in subtelomeres of haploid yeast. *J. Mol. Biol.*, **328**, 847–862.
 116. Mao, P., Liu, J., Zhang, Z., Zhang, H., Liu, H., Gao, S., Rong, Y.S. and Zhao, Y. (2016) Homologous recombination-dependent repair of telomeric DSBs in proliferating human cells. *Nat. Commun.*, **7**, 12154.
 117. Nelson, C.B., Alturki, T.M., Luxton, J.J., Taylor, L.E., Maranon, D.G., Muraki, K., Murnane, J.P. and Bailey, S.M. (2021) Telomeric double strand breaks in G1 human cells facilitate formation of 5' C-rich overhangs and recruitment of TERRA. *Front Genet.*, **12**, 644803.
 118. Schimmel, J., Kool, H., van Schendel, R. and Tijsterman, M. (2017) Mutational signatures of non-homologous and polymerase theta-mediated end-joining in embryonic stem cells. *EMBO J.*, **36**, 3634–3649.
 119. Yu, W., Lescale, C., Babin, L., Bedora-Faure, M., Lenden-Hasse, H., Baron, L., Demangel, C., Yelamos, J., Brunet, E. and Deriano, L. (2020) Repair of G1 induced DNA double-strand breaks in S-G2/M by alternative NHEJ. *Nat. Commun.*, **11**, 5239.
 120. Bhargava, R., Sandhu, M., Muk, S., Lee, G., Vaidehi, N. and Stark, J.M. (2018) C-NHEJ without indels is robust and requires synergistic function of distinct XLF domains. *Nat. Commun.*, **9**, 2484.
 121. Iliakis, G., Mladenov, E. and Mladenova, V. (2019) Necessities in the processing of DNA double strand breaks and their effects on genomic instability and cancer. *Cancers (Basel)*, **11**, 1671.
 122. Carvajal-Garcia, J., Cho, J.E., Carvajal-Garcia, P., Feng, W., Wood, R.D., Sekelsky, J., Gupta, G.P., Roberts, S.A. and Ramsden, D.A. (2020) Mechanistic basis for microhomology identification and genome scarring by polymerase theta. *Proc. Natl. Acad. Sci. U. S. A.*, **117**, 8476–8485.
 123. He, P. and Yang, W. (2018) Template and primer requirements for DNA Pol theta-mediated end joining. *Proc. Natl. Acad. Sci. U. S. A.*, **115**, 7747–7752.
 124. Kent, T., Chandramouly, G., McDevitt, S.M., Ozdemir, A.Y. and Pomerantz, R.T. (2015) Mechanism of microhomology-mediated end-joining promoted by human DNA polymerase theta. *Nat. Struct. Mol. Biol.*, **22**, 230–237.
 125. Chuang, S.M., Wang, L.H., Hong, J.H. and Lin, Y.W. (2008) Induction of Rad51 protein levels by p38 MAPK decreases cytotoxicity and mutagenicity in benzo[a]pyrene-exposed human lung cancer cells. *Toxicol. Appl. Pharmacol.*, **230**, 290–297.
 126. Ghadaouia, S., Olivier, M.A., Martinez, A., Kientega, T., Qin, J., Lambert-Lanteigne, P., Cardin, G.B., Autexier, C., Malaquin, N. and Rodier, F. (2021) Homologous recombination-mediated irreversible genome damage underlies telomere-induced senescence. *Nucleic Acids Res.*, **49**, 11690–11707.
 127. Hayashi, M.T., Cesare, A.J., Fitzpatrick, J.A., Lazzarini-Denchi, E. and Karlseder, J. (2012) A telomere-dependent DNA damage checkpoint induced by prolonged mitotic arrest. *Nat. Struct. Mol. Biol.*, **19**, 387–394.
 128. Glousker, G., Briod, A.S., Quadroni, M. and Lingner, J. (2020) Human shelterin protein POT1 prevents severe telomere instability induced by homology-directed DNA repair. *EMBO J.*, **39**, e104500.
 129. Kim, M.K. and Smith, S. (2014) Persistent telomere cohesion triggers a prolonged anaphase. *Mol. Biol. Cell.*, **25**, 30–40.
 130. Azarm, K., Bhardwaj, A., Kim, E. and Smith, S. (2020) Persistent telomere cohesion protects aged cells from premature senescence. *Nat. Commun.*, **11**, 3321.
 131. Mirman, Z., Lottersberger, F., Takai, H., Kibe, T., Gong, Y., Takai, K., Bianchi, A., Zimmermann, M., Durocher, D. and de Lange, T. (2018) 53BP1-RIF1-shieldin counteracts DSB resection through CST- and Polalpha-dependent fill-in. *Nature*, **560**, 112–116.
 132. Mirman, Z., Sasi, N.K., King, A., Chapman, J.R. and de Lange, T. (2022) 53BP1-shieldin-dependent DSB processing in BRCA1-deficient cells requires CST-Polalpha-primase fill-in synthesis. *Nat. Cell Biol.*, **24**, 51–61.
 133. Noordermeer, S.M., Adam, S., Setiapatra, D., Barazas, M., Pettitt, S.J., Ling, A.K., Olivieri, M., Alvarez-Quilon, A., Moatti, N., Zimmermann, M. *et al.* (2018) The shieldin complex mediates 53BP1-dependent DNA repair. *Nature*, **560**, 117–121.
 134. Shibata, A. and Jeggo, P.A. (2020) Roles for 53BP1 in the repair of radiation-induced DNA double strand breaks. *DNA Repair (Amst.)*, **93**, 102915.
 135. Dev, H., Chiang, T.W., Lescale, C., de Krijger, I., Martin, A.G., Pilger, D., Coates, J., Sczaniecka-Clift, M., Wei, W., Ostermaier, M. *et al.* (2018) Shieldin complex promotes DNA end-joining and counters homologous recombination in BRCA1-null cells. *Nat. Cell Biol.*, **20**, 954–965.
 136. Zatreanu, D., Robinson, H.M.R., Alkhatib, O., Boursier, M., Finch, H., Geo, L., Grande, D., Grinkevich, V., Heald, R.A., Langdon, S. *et al.* (2021) Poltheta inhibitors elicit BRCA-gene synthetic lethality and target PARP inhibitor resistance. *Nat. Commun.*, **12**, 3636.
 137. Biels, R., Steinlage, M., Barton, O., Juhász, S., Kunzel, J., Spies, J., Shibata, A., Jeggo, P.A. and Lobrich, M. (2017) DNA double-strand break resection occurs during non-homologous end joining in G1

- but is distinct from resection during homologous recombination. *Mol. Cell*, **65**, 671–684.
138. Ngo,G.H. and Lydall,D. (2015) The 9-1-1 checkpoint clamp coordinates resection at DNA double strand breaks. *Nucleic Acids Res.*, **43**, 5017–5032.
139. Carneiro,T., Khair,L., Reis,C.C., Borges,V., Moser,B.A., Nakamura,T.M. and Ferreira,M.G. (2010) Telomeres avoid end detection by severing the checkpoint signal transduction pathway. *Nature*, **467**, 228–232.
140. Desai,A., Yan,Y. and Gerson,S.L. (2018) Advances in therapeutic targeting of the DNA damage response in cancer. *DNA Repair (Amst.)*, **66-67**, 24–29.
141. Huang,R.X. and Zhou,P.K. (2020) DNA damage response signaling pathways and targets for radiotherapy sensitization in cancer. *Signal Transduct Target Ther*, **5**, 60.
142. Pilie,P.G., Tang,C., Mills,G.B. and Yap,T.A. (2019) State-of-the-art strategies for targeting the DNA damage response in cancer. *Nat. Rev. Clin. Oncol.*, **16**, 81–104.
143. Sprung,C.N., Afshar,G., Chavez,E.A., Lansdorp,P., Sabatier,L. and Murnane,J.P. (1999) Telomere instability in a human cancer cell line. *Mutat. Res.*, **429**, 209–223.
144. Sprung,C.N., Sabatier,L. and Murnane,J.P. (1999) Telomere dynamics in a human cancer cell line. *Exp. Cell. Res.*, **247**, 29–37.